Single-cell transcriptomics identifies a dampened neutrophil function and accentuated T-cell cytotoxicity in tobacco flavored e-cigarette exposed mouse lungs

Kaur G, PhD, Lamb T, PhD, Tjitropranoto A, and Irfan Rahman, PhD

[1]Department of Environmental Medicine, University of Rochester Medical Center, Rochester, NY, USA

Correspondence should be addressed to:

Irfan Rahman, Ph.D.
Department of Environmental Medicine
University of Rochester Medical Center
Box 850, 601 Elmwood Avenue
Rochester 14642, NY, USA
Tel: 1 585 275 6911
E-mail: irfan_rahman@urmc.rochester.edu
Irfan Rahman, PhD: ORCID # 0000-0003-2274-2454

Short running title: scRNA transcriptomics profiles of flavored e-cig aerosol

Abstract

E-cigarettes (e-cigs) are a public health concern for young adults due to their popularity and evidence for increased oxidative stress and immunotoxicity. Yet an extensive study defining the cell-specific immune changes upon exposure to flavored e-cigs remains elusive. To understand the immunological lung landscape upon acute nose-only exposure of C57BL/6J to flavored e-cig aerosols we performed single-cell RNA sequencing (scRNA seq). scRNA profiles of 71,725 cells were generated from control and treatment groups (n=2/sex/group). A distinct phenotype of Ly6G- neutrophils was identified in lungs exposed to tobacco flavored e-cig aerosol which demonstrated dampened IL-1 mediated and pattern recognition signaling as compared to air controls. Differential gene expression analyses identified dysregulation of T-cell mediated pro-inflammation (*Cct7*, *Cct8*) and stress-response signals (*Neurl3*, *Stap1*, *Cirbp* and *Htr2c)* in the lungs of mice exposed to e-cig aerosols, with pronounced effects for tobacco flavor. Flow cytometry analyses and cytokine/chemokine assessments within the lungs corroborated the scRNA seq data, demonstrating a significant increase in T-cell percentages and levels of T-cell associated cytokine/chemokines in the lungs of tobacco-flavored aerosol exposed mice. Increased levels of *Klra4* and *Klra8* expression also suggest an enhanced natural killer (NK) cell activity in this mouse group. Overall, this is a pilot study identifying increase in the percentages of Ly6G- neutrophils that may be responsible for dampened innate immune responses and heightened T-cell cytotoxicity in lungs of tobacco-flavored e-cig aerosol exposed mice. In addition, we provide preliminary evidence for sex-specific changes in the transcriptional landscape of mouse lungs upon exposure to e-cig aerosol, an area that warrants further study.

Keywords: E-cigarettes, Tobacco, scRNA seq, Immune cells, Innate immunity, Neutrophils, T-cells.

Introduction

Electronic cigarettes (e-cigs) or electronic nicotine delivery systems are a relatively novel set of tobacco and flavored products that have gained immense popularity amongst adolescents and young adults in the many countries including United States (US), United Kingdom (UK) and China. Flavors are one of the key features that make these products alluring to the younger diaspora (1). Reports indicate that in 2020 about 22.5% of high school students and 9.2% of middle school students in the US were daily vapers or e-cig users with fruit (66%), mint (57.5%), and menthol (44.5%) being the most preferred flavors (2). However, not much is known about the flavor-specific effects of e-cig vaping on the health and immunity of an individual.

E-cig products and aerosols are known to contain harmful constituents including formaldehyde, benzaldehyde, acrolein, n-nitrosamines, volatile organic compounds (VOCs), ketenes, and metal ions (3-5). Studies have indicated that exposure to e-cigs may enhance inflammatory responses, oxidative stress, and genomic instability in exposed cells or animal systems (6-8). Risk assessment of the non-carcinogenic (systemic) risks of inhaled diacetyl, a potential component of e-liquids, has estimated the hazard quotient to be greater than 1 amongst teens (9). Furthermore, clinical and *in vivo* studies have suggested that exposure to e-cig aerosols could impair innate immune responses in the host thus making them more susceptible to bacterial/viral

infections. The bacterial clearance, mucous production, and phagocytic responses in these individuals are shown to be affected upon use of e-cigs (10-14).

However, cell-specific changes within the lung upon vaping is not fully understood making it hard to determine the long-term health impacts of the use of these novel products. In this pilot study, we aim to determine effects of e-cig exposure on mouse lungs at single cell level. To do so, we exposed C57BL/6J mice to 5-day nose-only exposure to air, propylene glycol: vegetable glycerin (PG:VG), fruit-, menthol- and tobacco-flavored e-cig aerosols. We performed single-cell RNA sequencing (scRNA seq) on the lung digests from exposed and control animals and identified neutrophils and macrophages, among others, as the major cell populations in the lung that were affected upon acute exposure. We were able to identify 29 gene targets that were commonly dysregulated amongst all our treatment groups upon aggregating results from the major lung cell types identified in this study. These gene targets are the markers of early immune dysfunction upon e-cig aerosol exposure *in vivo* and could be studied in detail to understand temporal changes in their expression that may govern allergic responses and adverse pulmonary health outcomes upon acute and sub-acute exposures to e-cigarette aerosols.

Results

Fruit- flavored e-cig aerosol results in lung injurious responses upon acute exposure in vivo.

This study was designed to characterize the effects of exposure to flavored e-cig aerosol at single-cell level to understand the immunological changes in the lung

microenvironment upon e-cig use. To do so, we generated a first ever single-cell profile of e-cig aerosol exposed mouse lungs (n= 2/sex/group). The thus obtained results were then validated with the help of our validation cohort of n= 3/sex/group as shown in Fig 1A. Since all the commercially available e-liquids used in this study contained tobacco derived nicotine, we first determined the level of serum cotinine (a metabolite of nicotine) to prove successful exposure to the mice in each treatment group. As expected, we did not see any traces of cotinine in the serum of air and PG:VG exposed mice. Significant levels of cotinine were detected in the serum of mice exposed to fruit-, menthol-, and tobacco-flavored e-cig aerosols (Fig 1C).

Since metals released upon heating of the coils of e-cig devices are a source of toxicity upon vaping (15, 16), we further monitored the levels of metals in the e-cig aerosols generated during each day of mouse exposures. This acted as an indirect measure of characterizing the chemical properties of the aerosols used for exposure in this study. To monitor the release of metals into the lungs of the animals, the condensate from each day of exposure was collected and the levels of select elements were detected using ICP-MS. A detailed account of the concentrations of identified elements/metals is provided in Table 1. Interestingly, we identified flavor-dependent changes in the levels of metals like Ni, Zn, Na, K and Cu. Of note, despite the use of same wattage and temperature (max of 230ºC) for generation of e-cig aerosols, the leaching of each metal varied per day of exposure (Fig 1D). This is a crucial result as it highlights the importance of studying the impacts of coil composition and device design on the chemical composition of generated e-cig aerosols. These variations might affect the risk and toxicity associated with each of these products, an area that warrants further study.

Next, we performed H&E staining of the lung tissue sections to study the morphometric changes in the mouse lungs upon exposure to differently flavored e-cig aerosols. We did not find much evidence of tissue damage or airspace enlargement upon acute exposures in our model as expected. However, we found evidence of increased alveolar septa thickening in the lungs of both male and female mice exposed to fruit-flavored e-cig aerosols (Figure 1E). However, this could be a result of lower agarose inflation observed for the mouse lungs in this group of mice. We had challenges/difficulties with inflating the mouse lungs for all the mice in this group, however male mice showed more restriction than the female. Owing to the lack of proper inflation, the lungs were in a collapsed state than the other groups where the lungs were fully inflated. We have also performed mean linear intercept (Lm) measurements for all the lung tissue sections to show lowered Lm values for mouse lungs exposed to fruit-flavored e-cig aerosols as compared to air controls (Figure 1F). Airway obstruction could be indicative of "atelectasis", a condition that may result from lack of surfactant or alveolar damage thus affecting the lung expansion in these mice. Since this was not the prime focus of this study, we did not conduct further experiments to confirm out speculations, but nevertheless, we report these changes to inform and encourage further research in this area.

Detailed map of cellular composition during acute exposure to e-cig aerosols reveals distinct changes in immune cell phenotypes.

As the principle focus of this study was to identify the flavor-dependent and independent toxicities upon exposure to commercially available e-cig aerosols at the single-cell level, we performed the scRNA seq on the mouse lungs from exposed and control mice. After

quality control filtering (Figure S1), normalization and scaling, we generated scRNA seq profiles of 71,725 cells in total. Except for the PGVG group, all the rest of the treatments had approximately similar cell viabilities, cell capture, and other quality assessments in this study. However, for uniform analyses, equal features/ genes were used across all the groups for subsequent analyses. A detailed account of the cell viability, number of samples (single-cell capture)), and gene features identified before and after filtering upon QC check of sequenced data is provided in Table S1.

Uniform Manifold Approximation and Projection (UMAP) was used for dimensionality reduction and visualization of cell clusters. Cell annotations were performed based on the established cell markers in Tabula Muris database and available published literature. The general clustering of individual cell types based upon the commonly known cell markers was used to identify -**Endothelial** (identified by expression of *Cldn5*), **Epithelial** (identified by expression of *Sftpa1*), **Stromal** (identified by expression of *Col3a1*), and **Immune** (identified by expression of *Ptprc*) cells. The Immune cell population was further subclustered into lymphoid and myeloid populations in the UMAP analyses (Figure 2A&B). The relative cell percentages were plotted in a sex-dependent manner. Of note, upon assessing the sex- and treatment-specific changes in observed cell frequencies for individual cell types using two-way ANOVA, we did not find any significant variation in the relative frequencies of the general cell types in our treatment groups across both sexes (Figure 2C). A detailed account of the two-way ANOVA statistics for individual cell types is provided in Table S2.

DESeq2 was then used to identify the differentially regulated genes in each broad cell category. A list of significant ($p_{adj}<0.05$) differentially expressed genes (DEGs) was

generated using aggregate analysis for both sexes for each treatment group and number of up- and down-regulated genes were plotted in a flavor-dependent manner to get a snapshot of the cell-types and flavor-categories that show most dysregulation upon exposure (Figure 2D). Our data showed dysregulation of genes in endothelial, epithelial, and stromal cell populations, but maximum effect was observed on the cells from immune cell clusters. This is not surprising, as the immune system especially the myeloid cells form the frontline of the host's defenses against external stressors (17, 18). Compared to air, we observed a dysregulation of 553 genes (338 upregulated; 215 downregulated) in the myeloid cell cluster of mouse lungs exposed to tobacco-flavored e-cig aerosol. We identified 324 and 24 DEGs in the myeloid lung cluster from mouse lungs exposed to menthol- and fruit-flavored e-cig aerosols respectively as compared to air control. For the lymphoid cluster, we observed maximum dysregulation in the lungs exposed to fruit-flavored e-cig aerosols with a total of 112 DEGs. In contrast, 41 and 9 significant DEGs were identified for lymphoid cluster from lungs exposed to tobacco and menthol-flavored aerosols respectively.

It is important to mention here that most of the commercially available e-liquids /e-cig products use PG:VG as the base liquid to generate the aerosol and act as a carrier for flavoring chemicals. Thus, we compared the effect of PG:VG alone in our study to make further comparisons between individual flavoring products with that of PG:VG only. DESeq2 analyses showed dysregulation of 276 genes in mouse lungs exposed to PG:VG alone in the myeloid cell cluster as compared to air controls. Contrary to this, exposure to PG:VG aerosols affected 24 genes in the lymphoid cluster as compared to air control. Furthermore, when compared to PG:VG, exposure to fruit-flavored e-cig

aerosol dysregulated 262 genes in the myeloid cluster and 37 genes in the lymphoid cluster (Table 2).

Exposure to tobacco-flavored e-cig aerosols dampens IL-1 mediated signaling in Ly6G- neutrophil cluster.

We found maximum dysregulation in immune cell population, more specifically the myeloid cells, upon exposure to e-cig aerosols through our previous analyses. We thus subclustered the myeloid and lymphoid cell populations to further sub-divide their cell types and identify the flavor-dependent changes in immune cell responses. Upon sub clustering the myeloid cell population, we identified 14 unique clusters comprising all the major cell phenotypes including neutrophils, alveolar macrophages (AM), interstitial macrophages (IM), monocytes, dendritic cells (DC), and mast cells (Figure 3A). A detailed account of all the cell types identified with their respective marker genes is provided in Table 3. Cell cycle scoring revealed the neutrophil cluster to be in G2M phase (Figure 3B), indicating that these cell types are either at a checkpoint for uncontrolled proliferation or advancing toward a state of exhaustion (19, 20). In either case, we believed that studying these cells might be of interest to understand the mechanisms governing the immune dysregulation upon exposure of C57BL/6J mice to differently flavored e-cig aerosols. On deeper evaluation, we identified two unique phenotypes of neutrophils (identified by *S100a8*, *Cxcl2*, *Sell* and *Lcn2)* in the mouse lungs. These clusters were named as Ly6G^{+} Neutrophils and Ly6G^{-} Neutrophils based on the presence or absence of Ly6G marker, respectively (Figure 3C). Ly6G is important for neutrophil migration and is crucial to regulate neutrophil function within the lung (21). Interestingly we found a consistent flavor-dependent increase (though not

significant) in the Ly6G$^-$ neutrophil percentage in the lungs of exposed mice as compared to air controls. To validate the changes in cell percentages upon flavor exposure from scRNA seq, we performed flow cytometry. Our data from flow cytometry corroborated with the scRNA analyses results showing an increase in the levels of Ly6G+ neutrophils in lung digests from mouse lungs exposed to tobacco-flavored e-cig aerosols. The observed increase was more pronounced in males as compared to females thus highlighting the sex-dependent nature of changes in immune cell frequencies within the exposed lungs (Figure 3E).

AM form the bulk of the myeloid cell population in the lung and are characterized by top markers like *Chil3*, *Plet1*, *Lpl* and *Marco* (Figure 3C) (22). A flavor-dependent decrease in the resident AM (RAM) population was observed for both menthol and tobacco flavored e-cig aerosol exposed lungs (Figure 3D). These changes were again corroborated through the significant decrease in the BALF macrophage cell percentages in menthol-flavored e-cig aerosol exposed mice lungs as compared to air controls for both male and female mice (Figure 3F). Of note, though not significant, we saw a decrease in the levels of resident macrophages in the lung digests from mouse lungs exposed to menthol flavored e-cig aerosols with a more pronounced decrease observed amongst female mice (Figure S2A). Interestingly we found a distinct population of RAM expressing markers including *Mki67*, *Pclaf* and *Top2a*. These genes are responsible for cell proliferation. Importantly, the cell scoring for the G2M phase of the cell cycle was high for this cell cluster and thus these were labeled as ‘proliferating’ RAMs (pRAM) (23, 24). The pRAMs showed significant ($p=0.0156$) changes in the cell percentages with respect to varying exposures in our study (Figures 3D, Table S2).

Taken together, we show a significant shift towards the neutrophil-mediated immune response in the lungs of animals exposed to tobacco-flavored e-cig aerosols in our study. It is important to mention that due to the presence of nicotine in all the e-liquids used as treatment groups for this study, we added an extra control group- PGVG+Nic- for select experiments. Flow cytometric analyses revealed slight variations in the lung neutrophils and macrophage percentages observed in PGVG+Nic group as compared to PGVG only. However, none of these changes were significant. Furthermore, the patterns of change observed for the lungs exposed to aerosols from flavored e-liquids were quite distinct from those observed for PGVG+Nic thus proving that the observed changes are not solely due to the presence of nicotine in these treatment groups (Figures 3E-F, S1A).

Differential gene expression analyses on the myeloid cell cluster identified maximum gene dysregulation in myeloid cell cluster from mouse lungs exposed to tobacco-flavored e-cig aerosols. Interestingly, we did not observe major dysregulation in the gene expression for myeloid cell cluster in fruit-flavored e-cig exposed mouse lungs as compared to air controls. A total of 24 genes (17 upregulated; 7 downregulated) were differentially expressed in the myeloid clusters of lungs of animals exposed to fruit-flavored e-cig aerosols (Figure 4A). GO analyses identified terms like ‘myeloid cell differentiation’, ‘gas transport’ and ‘H_2O_2 catabolic process’ as the top hits for this cluster (Figures 4B). Importantly, few gene clusters (*Hbb-bs*, *Hbb-bt*, *Hba-a2* and *Hbb-a1*) showed sex-specific changes in the gene expressions in exposed lungs as compared to control. These genes clusters enrich for ‘erythrocyte development’ upon GO analyses and warrant further study.

We demonstrated an upregulation of 220 genes and a downregulation of 104 genes in the lungs of mice exposed to menthol-flavored e-cig aerosol as compared to ambient air. We observed increased expression of inflammatory genes including *Cxcl3*, *Il1r2, Stat4*, pointing towards the activation of chemokine-mediated signaling due to exposure to menthol-flavored e-cig aerosol. We also found a significant decrease in the expression of *Edn1* (endothelin1) in the myeloid cells of flavored e-cig aerosols as compared to air controls (Figure 4C). These genes play a role in positive regulation of neutrophil recruitment and inflammatory responses into the lungs (25-29). GO analyses of the DEGs ($p<0.01$), thus, showed 'cytokine-mediated signaling', 'cell chemotaxes', and 'negative regulation of MAPK cascade' as the top hits as shown in the Figure 4D.

Like menthol-, tobacco-flavored e-cig aerosol also elicited a significant increase in the expression of 338 genes and a decrease in 215 genes as compared to air controls in the myeloid cell cluster. We observed an increase in the expression of chemokines like *Stat4*, *Il1b*, and *Il1bos* in the myeloid cells resulting in terms like 'cytokine-mediated signaling pathway' enriched upon gene enrichment analyses. Like menthol-exposed mouse lungs, we found significant downregulation of Edn1 gene in the lungs of mice exposed to tobacco-flavored e-cig aerosol (Figure 4E). We provide the list of all DEGs as obtained from DESeq2 analyses and GO analyses results in Supplementary Excel Files 1-2.

Based on previous literature (30, 31) and enrichment of genes responsible for neutrophil chemotaxes in the current work, we reckoned this cell type to be of importance to be looked at separately *in vivo*. As mentioned earlier, we identified two distinct phenotypes of neutrophils- (a) $Ly6G^+$ neutrophils and (b) $Ly6G^-$ neutrophils. Interestingly, the

percentage increase in the Ly6G$^-$ neutrophil population of aerosol exposure was higher as compared to that for Ly6G$^+$ neutrophils per scRNA cell frequency analyses.

Upon performing DESeq2, we did not find any changes in the gene expressions for any of the two neutrophil populations for mouse lungs exposed to menthol-flavored e-cig aerosols despite an increase in the cell percentages of Ly6G- neutrophil phenotype. Interestingly, exposure to fruit-flavored e-cig aerosol caused most changes in the gene expressions in neutrophil population, with Ly6G$^-$ neutrophils being affected more than the Ly6G$^+$ population. We observed a dysregulation of 33 and 25 genes in Ly6G$^-$ neutrophil cluster from fruit- and PG:VG-aerosol exposed mouse lungs respectively. The Egl-9 Family Hypoxia Inducible Factor 3 (*Egln3*) gene was found to be downregulated upon exposure to e-cig aerosols in a flavor-independent manner. Egln3 has been known to play a crucial role in lung cancer and its inactivation exhibits lower tumor burden by induction of cancer senescence (32). We further identified dysregulation in the expressions of genes including *Irak2*, *Egr1, Il1r2*, *Pik3ap1*, and *Hspa8* in Ly6G$^-$ neutrophils for both fruit- and tobacco-aerosol exposed mouse lungs as compared to air controls. Furthermore, upregulation of genes like *Irak2* and *Egr1* in the Ly6G$^-$ neutrophils from mouse lungs exposed to PG:VG and fruit-flavored e-cig aerosol points towards the involvement of NF-κB mediated signaling in our study (Figure 4G). On performing gene enrichment analysis on the dysregulated gene sets from Ly6G- neutrophil cluster we obtained hits including ‘interleukin-1 mediated signaling pathway’, ‘hydrogen peroxide catabolic process’, and ‘pattern recognition signaling pathway’ (Supplementary Excel File 3). Of note, most of the associated genes were upregulated in lungs exposed to fruit-flavored e-cig aerosols. However, the expression pattern of

these gene sets points towards dampening of neutrophil-mediated immune responses for lungs exposed to tobacco-flavored e-cig aerosols as compared to air controls (Figure 4H). Compared to Ly6G$^-$ neutrophils, we did not observe any change in the gene expression profile of Ly6G$^+$ neutrophils for mouse lungs exposed to tobacco- flavored e-cig aerosol. For both, PG:VG and fruit-flavor e-cig aerosol exposed mouse lungs, *Treml4* (Triggering Receptor expressed on Myeloid Cells-Like Protein 4) gene was found to be downregulated in the Ly6G$^+$ neutrophils (Figure S2B). This gene functions as a positive regulator of TLR7 signaling (33, 34).

Activation of T-cell cytotoxic responses in lymphoid cells upon exposure to tobacco-flavored e-cig aerosols.

We identified 10 clusters upon sub clustering the lymphoid cell population. These comprised of: Pro-B cell, Pre-B cell, Mature B-cell, CD4+ T-cell, CD8+T-cell, Treg cell, AB T-cell, GD T-cell and Natural killer (NK) cells (35-37). Based on the expression of, *Ifit3*, *Oasl2* and *Rsad2* a unique cluster of IFN-stimulated B-cells was identified. The cell frequency of these cells was markedly lowered (19%) in mouse lungs exposed to tobacco-flavored e-cig aerosols as compared to air controls. Two-way ANOVA analysis of scRNA seq data showed significant changes ($p = 0.0237$) in the cell frequencies of CD4 T cells in a flavor-dependent manner in our treatment groups (Table S2). We also identified sex-dependent changes in the cell frequencies of B-cells ($p= 0.0148$), pro-B cells ($p= 0.0078$) and CD8 T cells ($p= 0.0265$) of the lymphoid cluster in our study (Figures 5A-C, Table S2). Flow cytometric analyses showed a significant increase in the CD4+ T-cell percentages in the lung digest from female mice exposed to tobacco-flavored e-cig aerosol. We also observed a significant increase in the CD8+ T cell

percentages in the lungs of tobacco-flavored e-cig aerosol exposed mice lungs as compared to air control in both male and female mice (Figure 5D). Of note, however, we found significant sex-dependent associations between the CD4+ T cell percentages (p= 0.0339) upon two-way ANOVA analyses of the flow cytometry data.

We found dysregulation of 112 genes (40 up- and 72-down-regulated) in mouse lungs exposed to fruit-flavored e-cig aerosols in the lymphoid cluster. We observe dysregulation of genes (*Incenp*, *Wnt4*, *Ccnb2*, *Trat1*, *Themis*) enriched for 'T-cell receptor signaling' and 'nuclear division', in exposed group as compared to air control (Figure 6A-B). Upregulation of genes like *Malt1* (Mucosa-associated lymphoid tissue lymphoma translocation protein 1), *Ppp1r2* (Protein phosphatase inhibitor 2), and *Spib* (Transcription factor Spi-B) indicates activation of T-cell mediated immune response upon exposure to fruit-flavored aerosol (38-40).

Contrary to the responses observed for exposure to fruit-flavored e-cig aerosols, we found significant upregulation in the expression of *Cdk8* and *Camk1d* genes in the lymphoid cell populations for menthol-flavored aerosol exposed mouse lungs (Figure 6C-D). *Cdk8* (cyclin-dependent kinase 8) is a transcriptional regulator that has a role in the cell cycle progression (41). Whereas *Camk1d* (calcium/calmodulin dependent protein kinase ID) functions to regulate calcium-mediated granulocyte function and respiratory burst within the cells(42). Taken together, our results point towards an increase in cell proliferation and gene transcription in the lymphoid cluster of mouse lungs exposed to menthol-flavored e-cig aerosols as indicated by enrichment of terms like 'cyclin-dependent protein serine/threonine kinase activity', 'RNA polymerase II CTD

modifying activity' and 'calmodulin-dependent protein kinase activity' associated with this cell cluster.

We observed the downregulation of genes responsible for chaperone-mediated protein folding (*Cct5*, *Cct7*, *Cct8*) in the lymphoid cells from tobacco-flavored e-cig aerosol exposed mouse lungs. Downregulation of these genes could be indicative of the accumulation of misfolded proteins in these lungs which may lead to enhanced cell death (43, 44). In fact, we found increased expression of killer cell lectin-like receptor (*Klra*)-4 and 8 in exposed mice lungs as compared to air controls, thus indicating that upon exposure to tobacco-flavored e-cig aerosols, the lymphoid cells undergo protein misfolding thereby resulting in increased cell death (Figure 6E-F). A detailed account of the DESeq2 results and GO analyses for all the groups is provided in Supplementary Excel files 4-5.

Dysregulation of chemokine signaling and T-cell activation on exposure to flavored e-cig aerosols.

Since we showed increased production of cytokines/chemokines, driving the immune responses in mouse lungs exposed to flavored e-cigs, we performed multianalyte assay to determine the levels of these inflammatory cytokines in the lung digests from the exposed animals as shown in Figure 7A. Exposure to tobacco-flavored e-cig aerosol resulted in a marked increase in the levels of chemotactic chemokines including CXCL16, CXCL12, CXC3R and proinflammatory cytokines including CCl12, CCL17, CCL24, and Eotaxin in the mouse lung digests as compared to air control. Supporting our transcriptional data, the levels of IL1b were dampened in the exposed mouse lungs thus showing negative regulation of IL-1 mediated signaling. We identified sex-

dependent changes in the cytokine levels in lung digests from fruit-flavored e-cig aerosols with male mice showing more dampening of cytokine/chemokine protein levels as compared to their female counterparts. Interestingly, the fold changes in the PGVG+Nic group were contrasting to those observed by PGVG alone and flavored e-cig aerosol exposed mouse lungs, again supporting our previous deduction that the observed changes are observed as a concerted effect of chemical present in the e-liquid used for flavored e-cig aerosol exposure.

To identify genes that were commonly dysregulated upon exposure, we generated a list of common genes that were significantly dysregulated in exposure categories (fruit, menthol and tobacco). We identified 9 such target genes-Ne*url3*, *Egfem1*, *Stap1*, *Tfec*, *Mitf*, *Cirbp*, *Hist1h1c*, *Gmds,* and *Htr2c* that were dysregulated in the myeloid cluster from lungs exposed to differently flavored e-cig aerosol, but not PGVG. We observed significant upregulation of *Neurl3*, *Stap1*, *Cirbp,* and *Hist1h1c* and downregulation of *Tfec*, *Mitf*, *Gmds,* and *Htr2c* in the myeloid cluster of mice exposed to differently flavored e-cig aerosol as compared to air control (Figure 7B). On analyzing the lymphoid cluster for commonly dysregulated genes, we identified - *Klra8* (Killer cell lectin-like receptor 8) and *Nfia* (nuclear factor I)- that were significantly upregulated in the exposure groups as compared to air-controls (Figure 7E). Klra8 is a natural killer cell associated gene, and its upregulation is generally associated with viral infection associated host immune responses within the mouse lungs (45-47). *Nfia* is a transcriptional activator responsible for regulating Oxphos-mediated mitochondrial responses and proinflammatory pathways (48, 49).

Overall, we identified a total of 29 commonly dysregulated gene targets were identified from five major cell clusters and performed gene enrichment analyses on the identified targets to identify the top hits (Tables 4-5). Terms like ‘negative regulation of immune system’ (*Hmgb3*/*Gpam*/*Scgb1a1*/*Stap1*/*Ldlr*), ‘positive regulation of lipid biosynthetic pathway’ (*Htr2c*/*Gpam*/*Ldlr*), and ‘receptor recycling’ (*Ldlr*/*Ramp3*) were amongst the top hits in our observations (Figure 7C).

Of note, the data presented in this study is a sub-part of a larger study. In addition to the groups mentioned in this manuscript, we also had two additional groups of Tobacco-Derived (TDN) and Tobacco-Free Nicotine (TFN). Though further objectives and experimentations performed in both these studies were varied, common air and PG:VG samples were used for analyses of cytokine/chemokine and cell count data as described in our recent publication(50).

Discussion

E-cigs and associated products have constantly been under scrutiny by the US Food and Drug Administration (FDA) due to public health concerns. In February 2020, FDA placed a regulation on all cartridge-based flavored e-cigs except for menthol and tobacco to reduce the use of e-cigs amongst adolescents and young adults. But it left a loophole for the sale of flavored (including menthol) disposable and open system e-cigs (1, 51). Importantly, most e-cig related bans in the US have happen at the state level, thus allowing differential levels of restrictions imposed on the premarket tobacco applications (PMTAs) and sales which defeats the purpose of limiting their accessibility to the general public (52, 53). Each year new products are introduced in the market with

newer device designs and properties, to lure the users (adults between the ages of 18-24 years) which makes it crucial to continue with the assessments of toxicity and health effects of e-cigs in an unbiased manner (54).

Numerous studies indicate increased oxidative stress, DNA damage, and loss of neutrophil function due to exposure to e-cig aerosols *in vitro* and *in vivo* (7, 30, 31, 50, 55, 56). However, we do not have much knowledge about the cell populations and biological signaling mechanisms that are most affected upon exposure to differently flavored e-cig aerosols. To bridge this gap in knowledge, we studied the transcriptional changes in the inflammatory responses due to acute (1-hr nose-only exposure including 120 puffs for 5-consecutive days) exposure to fruit-, menthol- and tobacco-flavored e-cig aerosols using single-cell technology.

Reports indicate that the release of metal ions due to the burning of metal coil is a major source of variation during e-cig exposures (57-59). A 2021 study reported the presence of 21 elements in the pod atomizers from different manufacturers identifying a high abundance of 11 elements including nickel, iron, zinc, and sodium amongst others (60). Previous studies have also shown the presence of similar elements in the e-cig aerosols which could have a possible adverse health effect on the vapers (15, 61). But more importantly, our study points towards a much graver issue, which pertains to the product design of the e-cig vapes. We believe that the aerosol composition varies based on the type of atomizer, coil resistance, coil composition, and chemical reactivity of the e-liquid being used. While much work is done on the chemical composition of the flavors and e-liquids, the other aspects of device design remain understudied and must be an area of research in the future. Another factor that may limit the interpretation of our results

pertains to the correlation between the leached metal and the observed transcriptional changes. Since our study provides proof of day-to-day variation in the leaching of metal ions from the same liquid using the same atomizer, it could be possible to develop a statistical model correlating the differential metal exposure to the gene expression changes. We do not conduct such analyses as this was not the focus of this work, but it is a possibility that could be explored in the future.

E-cig vaping has been known to affect the innate and adaptive immune responses among vapers (30, 62-64), but flavor-specific effects on immune function are not fully explored. While we expected to see flavor-dependent changes in our experiment, we did not anticipate observing interesting sex-dependent variation in the lung tissues at single-cell level. In this respect, recent studies show concurring evidence suggesting sex-specific changes in lung inflammation, mitochondrial damage, gene expression, and even DNA methylation in mice exposed to e-cig aerosols (65, 66).

One of the most interesting discoveries from our single-cell analyses was the identification of a new cluster of neutrophils that was called Ly6G- neutrophils in this study. While we observed an increase in the cell percentages of these cells in our treatment groups, little to no change in the gene expression was noted in this study which could be indicative of impaired function of these neutrophil population, a fate being reported by various previous studies pertaining to e-cig exposures (13, 62). In fact, our study identified this unique population and showed that IL-1 mediated responses were dampened in tobacco and menthol-exposed lung neutrophils which was corroborated by mild to no change in the levels of IL-1β in the lung tissue digests from exposed mice as compared to air. Ly6G is an important marker of neutrophil

maturation in mammalian cells and has been reported in relation to various bacterial and parasitic infections in previous studies (67, 68).Exposure to e-cig aerosols may result in a loss of function of mature neutrophils in the mouse lungs which gets actively replaced by inactive/immature neutrophils that are deficient in Ly6G expression. In fact, this could explain our inability to identify significant changes in mature neutrophil population through flow cytometry (where Ly6G was used as a marker) when comparing treated and control groups. Interestingly, our i*n vivo* findings were corroborated by a recently published work where neutrophils from healthy volunteers demonstrated a reduction in neutrophil chemotaxis, phagocytic function, and neutrophil extracellular trap formation on exposure to e-cig aerosols, thus suggesting loss of function by mature neutrophils (30). However, this study did not investigate the effects on the immature neutrophil population, an area that needs further study in future research.

Of note, myeloid and lymphoid limbs of immunity are interconnected (69, 70). A decline in the neutrophil-mediated immunity might activate other cell types to offer protection. In our study, we find a decline in the neutrophilic immune responses in menthol and tobacco flavored e-cig exposed mouse lungs. Contrarily, we report an increase in the T-cell responses in the form of increased CD4+ and CD8+ T cells from both scRNA seq and flow cytometric analyses. In fact, increased expression of genes including *Malt1*, *Serpinb9b,* and *Sema4c* are indicative of enhanced T-cell mediated immune response in the lungs of mice exposed to fruit(mango) flavored e-cig aerosols (71-73). Contrary to this, exposure to menthol-flavored e-cig aerosols had a much milder effect on the lymphoid population within the lungs of C57Bl/6J mice. We found evidence for increased cell proliferation due to activation of cyclin-dependent protein kinase signaling

mediated via expression of genes including *Cdk8* and *Camk1d* in these cells (42, 74). Exposure to tobacco-flavored e-cig aerosol provided evidence for decreased chaperone-mediated protein folding, due to the downregulation of Chaperonin Containing TCP-1 (CCT) family of proteins. Chaperonin Containing TCP-1 proteins are important to regulate the production of native active, tubulin, and other proteins crucial for cell cycle progression and cytoskeletal organization (75). This is in conjunction with the upregulation of *Klra4* and *Klra8* that is indicative of increased protein misfolding and cytotoxic responses in the lymphoid cells of tobacco-exposed e-cig aerosols (76, 77).

Overall, we provide evidence of subdued innate immune responses due to loss of function of neutrophils and increased T-cell proliferation and cytotoxicity in a flavor-dependent manner upon exposure to e-cig aerosols in this study. An increase in the levels of CCL17, CCL20, CCL22, IL2 and Eotaxin in the lung digests from tobacco-exposed mouse lungs further support this deduction as these cytokines/chemokines are associated with T-cell mediated immune responses (78-85). Importantly CXCL16 attracts T-cells and natural killer cells to activate cell death. It has been reported to be involved in LPS-mediated acute lung injury (ALI), an outcome which has also been linked with e-cig exposures in human (86, 87).

In the end, we compiled a list of commonly dysregulated genes in a flavor independent manner and identified 29 gene targets. Signal-transducing adaptor protein-2 (*Stap1)* which is commonly upregulated upon exposure to e-cig aerosols is known to regulate T-cell activation and airway inflammation which falls in line with the overall crux of our findings (88). Another gene that was found to be consistently dysregulated in many cell types was Cold-inducible RNA binding protein (*Cirbp*). *Cirbp* is a stress response

proteins linked with stressors like hypoxia. Its upregulation upon e-cig exposure supports that vaping induces oxidative stress and can have adverse implications on the exposed cell types (89). 5-hydroxytryptamine receptor 2C (*Htr2c*) and *Klra8* are other genes in this category of commonly dysregulated genes that are associated with enhancing inflammation and cell death (76, 77, 90). Overall, we provide a cell-specific atlas of immune responses upon exposure to differently flavored e-cig aerosols.

Considering that scRNA technology has not been commonly used for e-cig research, ours is one of the first studies employing this technique to identify possible changes in the cellular composition and gene expressions. Importantly we use the nose-only exposure system for our experiment to avoid exposure through other routes. However, despite the novel approach and state-of-the-art exposure system, we had a few limitations. First, we used a small sample size to identify the changes in the mouse lungs upon exposure to e-cig aerosols at a single-cell level. Due to the expensive nature of single-cell sequencing technology and limited information in the literature reporting changes at single-cell level, we chose to design this experiment with small sizes of experimental and validation cohort. But, based on the encouraging findings from this pilot study, future studies could be designed with a larger sample size and longer durations of exposure to identify the acute and chronic effects of vaping. Second, we could not delineate the sex-dependent changes upon exposure from our data. While we found evidence of sex-dependent differences in immune responses on exposure to differently flavored e-cig aerosols we pooled the samples from 2 mice/sex/group to perform scRNA seq analyses. This limits us from analyzing and drawing conclusions with regards to the sex-dependent variations at the level of differential gene expression

in our data with confidence. Thus, we chose to use aggregate analyses to make comparisons. However, future experimental designs must study sex as a confounder for studying the effects of e-cig exposure in humans. Third, the inclusion of PGVG+Nic group was streamlined in this study, but future work including this group for scRNA seq analyses might be crucial to delineate the effects of nicotine alone on gene transcription. Fourth, we did not anticipate changes in the metal release on consecutive days of exposure in our study. Our data pointed towards the importance of device design in e-cig exposures. Future studies need to identify the factors that may affect the daily composition of e-cig aerosols and devise a method of better monitoring these possible confounders. However, in this regard our experiment does mimic the real-life well, as such variations due to prolonged storage of e-liquid and differences arising due to vape design must be common amongst human vapers.

In conclusion, we identified cell-specific changes in the gene expressions upon exposure to e-cig aerosols using single cell technology. We identified a set of top 29 dysregulated genes that could be studied as markers of toxicity/immune dysfunction in e-cig research. Future work with larger sample sizes and sex-distribution is warranted to understand the health impacts of long-term use of these novel products in humans.

Methods

Animals Ethics Statement

All experiments were conducted per the guidelines set by the University Committee on Animal Resources at the University of Rochester Medical Center (URMC). Care was taken to implement an unbiased and robust approach during the experimental design

and conduction of each experiment to ensure data reproducibility per the National Institutes of Health standards.

Animals

We ordered 5-week-old pups of male and female C57BL/6J mice from Jackson Laboratory to conduct this experiment. Prior to the start of the experiment, mice were housed at the URMC Vivarium for acclimatization. Thereafter the animals were moved to the mouse Inhalation Facility at URMC for training and exposures.

One week prior to the start of the exposures, mice underwent a five-day nose-only training to adapt themselves to the mesh restraints of the exposure tower. The mouse restraint durations were increased gradually to minimize the animal stress and discomfort. Of note, the mouse sacrifice was performed within 8-12 weeks' age for each mouse group to ensure that the mouse age corresponds to the age of adolescents (12-17 years) in humans (91, 92).

E-cigarette Device and E-liquid

We utilized an eVic-VTC mini and CUBIS pro atomizer (SCIREQ, Montreal, Canada) with a BF SS316 1.0-ohm coil from Joyetech (Joyetech, Shenzhen, China) for vaping and the inExpose nose-only inhalation system from SCIREQ (SCIREQ, Montreal, Canada) for mouse exposures. Both air and PG:VG exposed mice groups were considered as controls for this experiment. We used commercially available propylene glycol (PG; EC Blend) and vegetable glycerin (VG; EC Blend) in equal volume to prepare a 50:50 solution of PG:VG. For flavored product exposures, mice were exposed to three different e-liquids – a menthol flavor "Menthol-Mint", a fruit flavor "Mango" and a

tobacco flavor “Cuban Blend”. Of note, all the e-liquids were commercially manufactured with 50mg/mL of tobacco derived nicotine (TDN). So, all treatments have nicotine in addition to the flavoring mentioned respectively. Additionally, we used a mixture of PG:VG with 50mg/mL of TDN as a control for limited experiments to study the effect of nicotine alone in our treatment. This group is labeled as PGVG+Nic for the rest of the manuscript.

E-cigarette Exposure

Scireq Flexiware software with the InExpose Inhalation system was used for controlling the Joyetech eVic-VTC mini device to perform nose-only mouse exposures. For this exposure, we utilized a puffing profile that mimicked the puffing topography of e-cig users in two puffs per minute with a puff volume of 51 mL, puff duration of 3 seconds, and an inter puff interval of 27 seconds with a 2 L/min bias flow between puffs (93). Figures 1A and 1B depict the experimental design and exposure system employed for this study.

Age-matched male and female (n=5 per sex) mice were used for each group, namely, air, PG:VG, Fruit, Menthol, and Tobacco. To ensure rigor and reproducibility in our work, we have used age- and sex-matched control and treated mice in this study. Confounders like environment and stress were minimized by housing all the cages in environmentally controlled conditions and training all the mice (both control and treated) in nose-only chambers. Each group of mice was exposed to the above-mentioned puffing profile for one hour each day (120 puffs) for a total of five consecutive days. Additionally, a group of mice (n=3/sex) was exposed to PGVG+Nic for the same duration using similar exposure profile to serve as control to assess the effect of

nicotine on the observed changes using selected experiments. Air-exposed mice were exposed to the same puffing profile for a total of five consecutive days to ambient air. We recorded the temperature, humidity, and CO levels of the aerosols generated at the start, mid, and end of the exposure on each day using the Q-Trak Indoor Air Quality Monitor 7575 (TSI, Shoreview, MN). Total Particulate Matter (TPM) sampling was done from the exhaust tubing of the set-up at the 30 min mark of the exposure and at the inlet connected to the nose-only tower (shown in Figure 1B) immediately after the culmination of the exposure. Gravimetric measurements for TPM were also conducted to confirm relative dosage to each mouse group daily.

Preparation of single-cell suspension

The animals were sacrificed (at 8-10 weeks' age) immediately after the final exposure. Vascular lung perfusion was performed using 3mL of saline before harvesting the lung lobes for preparation of single-cell suspension. It is important to mention here that of the 5 lung samples/sex/group; 2 sex/group were used for histological assessments and scRNA analyses. Here, the left lung lobe was inflated using low-melting agarose and used for histology, while the rest of the uninflated lung lobes were used for preparing the single-cell suspension. We pooled the lung lobes for each sex per group for preparation of the single-cell suspension as depicted in Figure 1A. The lung lobes were weighed digested using Liberase method as described earlier(94).

Library Preparation and Single-Cell Sequencing

The prepared single-cell suspension was sent to the Genomics Research Center (GRC) at URMC for library preparation and single-cell sequencing. Library preparation was performed from control and treatment groups using the 10X single-cell sequencing

pipeline by 10X Genomics and 10000 cells were captured per sample using the Chromium platform. The prepared library was sequenced on NovaSeq 6000 (Illumina, San Diego, CA) at a mean sequence depth of 30,000 reads per cell. Read alignment was performed to GRCm38 Sequence.

Data Analyses

We used the standard Seurat v4.2 analyses pipeline to analyze our data (95). In brief the low-quality cells and potential doublets were excluded from the dataset to create the analyses dataset. The residual features due to the presence of RBCs were corrected before integration. “scTransform” function was used for integration of all the datasets after which the standard Seurat pipeline was used for data normalization of integrated data. “FindVariableGenes” gene function was used to identify the variable genes for dimensionality reduction using PCA function. UMAP was used for dimensionality reduction and clustering of the cells.

To identify the unique features and cell clusters within each cell subtypes, we used the sub-setting feature within Seurat. After identifying the 5 major cell populations (epithelial, endothelial, stromal, myeloid and lymphoid) in our data sets, each of these cell types were sub-clustered using “subset ()” function, normalized and re-clustered. Cell annotation for each of the subsets was performed with the help of Tabula Muris database (35, 96). However, some clusters were annotated manually with the help of a literature search as discussed in the results section.

DESeq2 (97) was used to perform pseudobulk analyses to identify differentially expressed genes within each group. The ClusterProfiler (98) was employed to perform gene enrichment analyses of the differentially expressed genes.

Cytokine/chemokine assessment

We used multiplex assay to determine the levels of cytokine/chemokine in the lung homogenates from control and e-cig aerosol exposed mouse lungs using commercially available Bio-Plex Pro Mouse Chemokine Assay (Cat#12009159, Bio-RAD, Hercules, CA) per the manufacturer's instructions. Approximately 40 mg of mouse lung lobes were homogenized in 300uL of 1X RIPA buffer with 0.1% protease and phosphatase inhibitor. The lung homogenate was stored on ice for 30 min. Following incubation, the homogenate was centrifuged at 15000 rpm for 15 min at 4 degrees Celsius. The supernatant was collected and used for performing the multianalyte assay for determination of cytokine/chemokine levels using Luminex FlexMap3D system

Lung Histology

The left lung lobe of mice used for scRNA seq were inflated with 1% low melting agarose and fixed with 4% neutral buffered PFA. Fixed lungs were dehydrated, before being paraffin-embedded and sectioned (5μm). Hematoxylin and eosin (H&E) staining was performed by the Histology, Biochemistry, and Molecular Imaging Core at URMC. We employed MetaMorph software (Molecular Devices) to determine the "Mean linear intercept" (Lm) of airspace. In brief, 6-10 randomly selected ×100 fields per slide were photographed in a blinded manner, and Lm values were quantitated for each captured image using the MetaMorph software. Care was taken to avoid pictures with bronchiolar

regions and knife marks in the tissue for quantitation. An average of all quantified images was then plotted for each sample in a sex-dependent manner.

Flow cytometry

Flow cytometry was performed on the cells collected from BALF and lung homogenates from air and flavored e-cig aerosol exposed mouse lungs. For analyses of cells collected from BALF, the fluid was centrifuged at 2000g for 10 min at 4^0C. Supernatant was collected for ELISA, while the cell pellet was re-suspended in 1mL of PBS. For analyses of immune cell population in the lung, the lung lobes were digested as described earlier (94) . The single-cell suspension thus prepared was used to run flow cytometry using the BD LSRFortessa cell analyzer. Cells were blocked with CD16/32 (Tonbo biosciences 70-0161-u500, 1:10) to prevent nonspecific binding and stained with a master mix of Siglec F (BD OptiBuild Cat#740280, 1:200), CD11b (Biolegend Cat #101243, 1:200), Ly6G (BD Horizon Cat# 562700, 1:200), CD45 (Biolegend Cat#103126, 1:200), CD11c (Biolegend Cat #117318, 1:200), CD4 (Biolegend Cat#116012, 1:200), and CD8 (eBiosciences Cat#17-0081-82, 1:200). 7AAD (eBiosciences Cat#00-6993-50, 1:10) was used as the nucleic acid dye to detect live and dead cells.

Metal analyses

To understand the levels of metals released during subsequent days of exposure, we performed Inductively coupled plasma mass spectrometry (ICP-MS) on the e-cig aerosol condensates collected from each day of exposure using a Perkin Elmer ICP-MS model 2000C. The samples were run using a Total Quant KED protocol with 4mL/min

Helium flow and externally calibrated using a blank and a 100ppb standard for the 51 elements. The samples were submitted to the Element Analyses facility at URMC, and levels of metals thus detected were plotted.

Statistical significance

We used GraphPad Prism 10.0 for all statistical calculations. All the data plotted in this paper are expressed as mean ± SEM. Pairwise comparisons were done using unpaired *t* test while one-way analysis of variance (ANOVA) with ad-hoc Tukey's test was employed for multi-group comparisons. To identify sex-based variations in our treatment groups, Tukey post hoc two-way ANOVA was employed.

Data Availability: The datasets generated during and/or analyzed during the current study are deposited on NCBI Gene Expression Omnibus. Specifically, mouse scRNAseq is available under accession code “GSE263903” (https://www.ncbi.nlm.nih.gov/geo/query/acc.cgi?acc=GSE263903). The data will be publicly available upon publication or on April 11, 2025, whichever is earlier. Reviewer’s token for access is ‘wtofqmayjdeltcn’. All other relevant data supporting the key findings of this study are available within the article and its Supplementary Information files or from the corresponding author upon reasonable request. Source data are provided with this paper.

Code Availability: Data collection was performed with mkfastq pipeline in Cell Ranger’s (v7.0.1). Cell Ranger (v7.0.1) was used for cell and gene counting using the default settings. Single-cell analysis was performed using the Seurat R package (v4.3.0) using the recommended workflow.

Author's contributions: GK, TL and AT planned and conducted the experiments; TL analyzed the lab-based assays; GK and AT analyzed the scRNA data; GK wrote and edited the manuscript; TL, AT and IR reviewed the data and manuscript; IR conceived and procured funding for the project.

Acknowledgements & Funding Sources: We would like to thank the Genomics Research Core, the Elemental Analyses Facility, and the Histology, Biochemistry, and Molecular Imaging Core at URMC for assisting us in the scRNA seq, metal analyses in aerosols, and lung sectioning and histology respectively. We would also like to acknowledge Chengru Jiang for helping with histology image acquisition for this manuscript. This work was supported by WNY Center for Research on Flavored Tobacco Products (CRoFT) # U54CA228110 and Toxicology Training Program grant T32 ES007026.

Conflict of Interest: The authors have no financial disclosure or conflict of interest with the findings presented in this research article.

References

1. Ma S, Qiu Z, Yang Q, Bridges JFP, Chen J, Shang C. Expanding the E-Liquid Flavor Wheel: Classification of Emerging E-Liquid Flavors in Online Vape Shops. Int J Environ Res Public Health. 2022;19(21).
2. Wang TW, Neff LJ, Park-Lee E, Ren C, Cullen KA, King BA. E-cigarette Use Among Middle and High School Students - United States, 2020. MMWR Morb Mortal Wkly Rep. 2020;69(37):1310-2.
3. Wu D, O'Shea DF. Potential for release of pulmonary toxic ketene from vaping pyrolysis of vitamin E acetate. Proc Natl Acad Sci U S A. 2020;117(12):6349-55.
4. Goniewicz ML, Kuma T, Gawron M, Knysak J, Kosmider L. Nicotine levels in electronic cigarettes. Nicotine Tob Res. 2013;15(1):158-66.
5. Lee YJ, Na CJ, Botao L, Kim KH, Son YS. Quantitative insights into major constituents contained in or released by electronic cigarettes: Propylene glycol, vegetable glycerin, and nicotine. Sci Total Environ. 2020;703:134567.
6. Wang Q, Sundar IK, Blum JL, Ratner JR, Lucas JH, Chuang TD, et al. Prenatal Exposure to Electronic-Cigarette Aerosols Leads to Sex-Dependent Pulmonary Extracellular-Matrix Remodeling and Myogenesis in Offspring Mice. Am J Respir Cell Mol Biol. 2020;63(6):794-805.

7. Muthumalage T, Lamb T, Friedman MR, Rahman I. E-cigarette flavored pods induce inflammation, epithelial barrier dysfunction, and DNA damage in lung epithelial cells and monocytes. Sci Rep. 2019;9(1):19035.
8. Lee HW, Park SH, Weng MW, Wang HT, Huang WC, Lepor H, et al. E-cigarette smoke damages DNA and reduces repair activity in mouse lung, heart, and bladder as well as in human lung and bladder cells. Proc Natl Acad Sci U S A. 2018;115(7):E1560-e9.
9. White AV, Wambui DW, Pokhrel LR. Risk assessment of inhaled diacetyl from electronic cigarette use among teens and adults. Sci Total Environ. 2021;772:145486.
10. Martin EM, Clapp PW, Rebuli ME, Pawlak EA, Glista-Baker E, Benowitz NL, et al. E-cigarette use results in suppression of immune and inflammatory-response genes in nasal epithelial cells similar to cigarette smoke. Am J Physiol Lung Cell Mol Physiol. 2016;311(1):L135-44.
11. Sussan TE, Gajghate S, Thimmulappa RK, Ma J, Kim JH, Sudini K, et al. Exposure to electronic cigarettes impairs pulmonary anti-bacterial and anti-viral defenses in a mouse model. PLoS One. 2015;10(2):e0116861.
12. Masso-Silva JA, Moshensky A, Shin J, Olay J, Nilaad S, Advani I, et al. Chronic E-Cigarette Aerosol Inhalation Alters the Immune State of the Lungs and Increases ACE2 Expression, Raising Concern for Altered Response and Susceptibility to SARS-CoV-2. Front Physiol. 2021;12:649604.
13. Madison MC, Landers CT, Gu BH, Chang CY, Tung HY, You R, et al. Electronic cigarettes disrupt lung lipid homeostasis and innate immunity independent of nicotine. J Clin Invest. 2019;129(10):4290-304.
14. Cao Y, Wu D, Ma Y, Ma X, Wang S, Li F, et al. Toxicity of electronic cigarettes: A general review of the origins, health hazards, and toxicity mechanisms. Sci Total Environ. 2021;772:145475.
15. Olmedo P, Goessler W, Tanda S, Grau-Perez M, Jarmul S, Aherrera A, et al. Metal Concentrations in e-Cigarette Liquid and Aerosol Samples: The Contribution of Metallic Coils. Environ Health Perspect. 2018;126(2):027010.
16. Aherrera A, Lin JJ, Chen R, Tehrani M, Schultze A, Borole A, et al. Metal Concentrations in E-Cigarette Aerosol Samples: A Comparison by Device Type and Flavor. Environ Health Perspect. 2023;131(12):127004.
17. Del Fresno C, Sancho D. Myeloid cells in sensing of tissue damage. Curr Opin Immunol. 2021;68:34-40.
18. Marshall JS, Warrington R, Watson W, Kim HL. An introduction to immunology and immunopathology. Allergy Asthma Clin Immunol. 2018;14(Suppl 2):49.
19. Gire V, Dulic V. Senescence from G2 arrest, revisited. Cell Cycle. 2015;14(3):297-304.
20. Oshi M, Takahashi H, Tokumaru Y, Yan L, Rashid OM, Matsuyama R, et al. G2M Cell Cycle Pathway Score as a Prognostic Biomarker of Metastasis in Estrogen Receptor (ER)-Positive Breast Cancer. Int J Mol Sci. 2020;21(8).
21. Lee PY, Wang JX, Parisini E, Dascher CC, Nigrovic PA. Ly6 family proteins in neutrophil biology. J Leukoc Biol. 2013;94(4):585-94.
22. Mould KJ, Jackson ND, Henson PM, Seibold M, Janssen WJ. Single cell RNA sequencing identifies unique inflammatory airspace macrophage subsets. JCI Insight. 2019;4(5).
23. Liégeois M, Bai Q, Fievez L, Pirottin D, Legrand C, Guiot J, et al. Airway Macrophages Encompass Transcriptionally and Functionally Distinct Subsets Altered by Smoking. Am J Respir Cell Mol Biol. 2022;67(2):241-52.
24. Woldemeskel M, Hawkins I, Whittington L. Ki-67 protein expression and tumor associated inflammatory cells (macrophages and mast cells) in canine colorectal carcinoma. BMC Vet Res. 2017;13(1):111.

775 25. Sokulsky LA, Garcia-Netto K, Nguyen TH, Girkin JLN, Collison A, Mattes J, et al. A Critical Role for
776 the CXCL3/CXCL5/CXCR2 Neutrophilic Chemotactic Axis in the Regulation of Type 2 Responses in a
777 Model of Rhinoviral-Induced Asthma Exacerbation. J Immunol. 2020;205(9):2468-78.
778 26. Metzemaekers M, Gouwy M, Proost P. Neutrophil chemoattractant receptors in health and
779 disease: double-edged swords. Cell Mol Immunol. 2020;17(5):433-50.
780 27. Tolomeo M, Cascio A. STAT4 and STAT6, their role in cellular and humoral immunity and in
781 diverse human diseases. Int Rev Immunol. 2024:1-25.
782 28. Boraschi D, Italiani P, Weil S, Martin MU. The family of the interleukin-1 receptors. Immunol
783 Rev. 2018;281(1):197-232.
784 29. Orsini EM, Perelas A, Southern BD, Grove LM, Olman MA, Scheraga RG. Stretching the Function
785 of Innate Immune Cells. Front Immunol. 2021;12:767319.
786 30. Jasper AE, Faniyi AA, Davis LC, Grudzinska FS, Halston R, Hazeldine J, et al. E-cigarette vapor
787 renders neutrophils dysfunctional due to filamentous actin accumulation. J Allergy Clin Immunol.
788 2024;153(1):320-9.e8.
789 31. Corriden R, Moshensky A, Bojanowski CM, Meier A, Chien J, Nelson RK, Crotty Alexander LE. E-
790 cigarette use increases susceptibility to bacterial infection by impairment of human neutrophil
791 chemotaxis, phagocytosis, and NET formation. Am J Physiol Cell Physiol. 2020;318(1):C205-c14.
792 32. Jin Y, Pan Y, Zheng S, Liu Y, Xu J, Peng Y, et al. Inactivation of EGLN3 hydroxylase facilitates Erk3
793 degradation via autophagy and impedes lung cancer growth. Oncogene. 2022;41(12):1752-66.
794 33. Gonzalez-Cotto M, Guo L, Karwan M, Sen SK, Barb J, Collado CJ, et al. TREML4 Promotes
795 Inflammatory Programs in Human and Murine Macrophages and Alters Atherosclerosis Lesion
796 Composition in the Apolipoprotein E Deficient Mouse. Front Immunol. 2020;11:397.
797 34. Nedeva C, Menassa J, Duan M, Liu C, Doerflinger M, Kueh AJ, et al. TREML4 receptor regulates
798 inflammation and innate immune cell death during polymicrobial sepsis. Nat Immunol.
799 2020;21(12):1585-96.
800 35. Hurskainen M, Mižíková I, Cook DP, Andersson N, Cyr-Depauw C, Lesage F, et al. Single cell
801 transcriptomic analysis of murine lung development on hyperoxia-induced damage. Nat Commun.
802 2021;12(1):1565.
803 36. Le Berre L, Chesneau M, Danger R, Dubois F, Chaussabel D, Garand M, Brouard S. Connection of
804 BANK1, Tolerance, Regulatory B cells, and Apoptosis: Perspectives of a Reductionist Investigation. Front
805 Immunol. 2021;12:589786.
806 37. Yang J, Ren J, Yang Y, Sun J, Zhou X, Zheng S, et al. BANK1 alters B cell responses and influences
807 the interactions between B cells and induced T regulatory cells in mice with collagen-induced arthritis.
808 Arthritis Res Ther. 2018;20(1):9.
809 38. O'Neill TJ, Tofaute MJ, Krappmann D. Function and targeting of MALT1 paracaspase in cancer.
810 Cancer Treat Rev. 2023;117:102568.
811 39. Horsnell HL, Cao WH, Belz GT, Mueller SN, Alexandre YO. The transcription factor SpiB regulates
812 the fibroblastic reticular cell network and CD8(+) T-cell responses in lymph nodes. Immunol Cell Biol.
813 2024;102(4):269-79.
814 40. Luo W, Xu C, Phillips S, Gardenswartz A, Rosenblum JM, Ayello J, et al. Protein phosphatase 1
815 regulatory subunit 1A regulates cell cycle progression in Ewing sarcoma. Oncotarget. 2020;11(19):1691-
816 704.
817 41. Dannappel MV, Sooraj D, Loh JJ, Firestein R. Molecular and in vivo Functions of the CDK8 and
818 CDK19 Kinase Modules. Front Cell Dev Biol. 2018;6:171.
819 42. Jin Q, Zhao J, Zhao Z, Zhang S, Sun Z, Shi Y, et al. CAMK1D Inhibits Glioma Through the
820 PI3K/AKT/mTOR Signaling Pathway. Front Oncol. 2022;12:845036.

821 43. Vallin J, Grantham J. The role of the molecular chaperone CCT in protein folding and mediation
822 of cytoskeleton-associated processes: implications for cancer cell biology. Cell Stress Chaperones.
823 2019;24(1):17-27.
824 44. Haeri M, Knox BE. Endoplasmic Reticulum Stress and Unfolded Protein Response Pathways:
825 Potential for Treating Age-related Retinal Degeneration. J Ophthalmic Vis Res. 2012;7(1):45-59.
826 45. Lopes N, Galluso J, Escalière B, Carpentier S, Kerdiles YM, Vivier E. Tissue-specific transcriptional
827 profiles and heterogeneity of natural killer cells and group 1 innate lymphoid cells. Cell Rep Med.
828 2022;3(11):100812.
829 46. Pommerenke C, Wilk E, Srivastava B, Schulze A, Novoselova N, Geffers R, Schughart K. Global
830 transcriptome analysis in influenza-infected mouse lungs reveals the kinetics of innate and adaptive host
831 immune responses. PLoS One. 2012;7(7):e41169.
832 47. Akter S, Chauhan KS, Dunlap MD, Choreño-Parra JA, Lu L, Esaulova E, et al. Mycobacterium
833 tuberculosis infection drives a type I IFN signature in lung lymphocytes. Cell Rep. 2022;39(12):110983.
834 48. Kong S, Chen TX, Jia XL, Cheng XL, Zeng ML, Liang JY, et al. Cell-specific NFIA upregulation
835 promotes epileptogenesis by TRPV4-mediated astrocyte reactivity. J Neuroinflammation.
836 2023;20(1):247.
837 49. Hiraike Y, Saito K, Oguchi M, Wada T, Toda G, Tsutsumi S, et al. NFIA in adipocytes reciprocally
838 regulates mitochondrial and inflammatory gene program to improve glucose homeostasis. Proc Natl
839 Acad Sci U S A. 2023;120(31):e2308750120.
840 50. Lamb T, Kaur G, Rahman I. Tobacco-Derived and Tobacco-Free Nicotine cause differential
841 inflammatory cell influx and MMP9 in mouse lung. Res Sq. 2023.
842 51. Sindelar JL. Regulating Vaping - Policies, Possibilities, and Perils. N Engl J Med. 2020;382(20):e54.
843 52. Bhalerao A, Sivandzade F, Archie SR, Cucullo L. Public Health Policies on E-Cigarettes. Curr
844 Cardiol Rep. 2019;21(10):111.
845 53. Azagba S, Ebling T, Adekeye OT, Hall M, Jensen JK. Loopholes for Underage Access in E-Cigarette
846 Delivery Sales Laws, United States, 2022. Am J Public Health. 2023;113(5):568-76.
847 54. N KEaE. Current Electronic Cigarette Use Among

848 Adults Aged 18 and Over: United States, 2021 2023.
849 55. Lamb T, Muthumalage T, Rahman I. Pod-based menthol and tobacco flavored e-cigarettes cause
850 mitochondrial dysfunction in lung epithelial cells. Toxicol Lett. 2020;333:303-11.
851 56. Ren X, Lin L, Sun Q, Li T, Sun M, Sun Z, Duan J. Metabolomics-based safety evaluation of acute
852 exposure to electronic cigarettes in mice. Sci Total Environ. 2022;839:156392.
853 57. Zhao D, Aravindakshan A, Hilpert M, Olmedo P, Rule AM, Navas-Acien A, Aherrera A.
854 Metal/Metalloid Levels in Electronic Cigarette Liquids, Aerosols, and Human Biosamples: A Systematic
855 Review. Environ Health Perspect. 2020;128(3):36001.
856 58. Zhao D, Navas-Acien A, Ilievski V, Slavkovich V, Olmedo P, Adria-Mora B, et al. Metal
857 concentrations in electronic cigarette aerosol: Effect of open-system and closed-system devices and
858 power settings. Environ Res. 2019;174:125-34.
859 59. Alcantara C, Chaparro L, Zagury GJ. Occurrence of metals in e-cigarette liquids: Influence of coils
860 on metal leaching and exposure assessment. Heliyon. 2023;9(3):e14495.
861 60. Omaiye EE, Williams M, Bozhilov KN, Talbot P. Design features and elemental/metal analysis of
862 the atomizers in pod-style electronic cigarettes. PLoS One. 2021;16(3):e0248127.
863 61. Rastian B, Wilbur C, Curtis DB. Transfer of Metals to the Aerosol Generated by an Electronic
864 Cigarette: Influence of Number of Puffs and Power. Int J Environ Res Public Health. 2022;19(15).
865 62. Kalininskiy A, Kittel J, Nacca NE, Misra RS, Croft DP, McGraw MD. E-cigarette exposures,
866 respiratory tract infections, and impaired innate immunity: a narrative review. Pediatr Med. 2021;4.

867 63. Rebuli ME, Glista-Baker E, Hoffman JR, Duffney PF, Robinette C, Speen AM, et al. Electronic-
868 Cigarette Use Alters Nasal Mucosal Immune Response to Live-attenuated Influenza Virus. A Clinical Trial.
869 Am J Respir Cell Mol Biol. 2021;64(1):126-37.
870 64. Reidel B, Radicioni G, Clapp PW, Ford AA, Abdelwahab S, Rebuli ME, et al. E-Cigarette Use
871 Causes a Unique Innate Immune Response in the Lung, Involving Increased Neutrophilic Activation and
872 Altered Mucin Secretion. Am J Respir Crit Care Med. 2018;197(4):492-501.
873 65. Song MA, Kim JY, Gorr MW, Miller RA, Karpurapu M, Nguyen J, et al. Sex-specific lung
874 inflammation and mitochondrial damage in a model of electronic cigarette exposure in asthma. Am J
875 Physiol Lung Cell Mol Physiol. 2023;325(5):L568-l79.
876 66. Chirumamilla P, Rousselle, D, Sharma, S, Commodore, S and Silveyra, P. Evaluation of Sex
877 Differences in DNA Methylation and Lung Tissue Gene Expression in a Mouse Model of E-cigarette
878 Exposure. Respiratory Physiology. 2024;39(S1).
879 67. Deniset JF, Surewaard BG, Lee WY, Kubes P. Splenic Ly6G(high) mature and Ly6G(int) immature
880 neutrophils contribute to eradication of S. pneumoniae. J Exp Med. 2017;214(5):1333-50.
881 68. Kleinholz CL, Riek-Burchardt M, Seiß EA, Amore J, Gintschel P, Philipsen L, et al. Ly6G deficiency
882 alters the dynamics of neutrophil recruitment and pathogen capture during Leishmania major skin
883 infection. Scientific Reports. 2021;11(1):15071.
884 69. Shanker A, Marincola FM. Cooperativity of adaptive and innate immunity: implications for
885 cancer therapy. Cancer Immunol Immunother. 2011;60(8):1061-74.
886 70. Carroll MC, Prodeus AP. Linkages of innate and adaptive immunity. Curr Opin Immunol.
887 1998;10(1):36-40.
888 71. Wang R, Zhang H, Xu J, Zhang N, Pan T, Zhong X, et al. MALT1 Inhibition as a Therapeutic
889 Strategy in T-Cell Acute Lymphoblastic Leukemia by Blocking Notch1-Induced NF-κB Activation. Front
890 Oncol. 2020;10:558339.
891 72. Bird CH, Christensen ME, Mangan MS, Prakash MD, Sedelies KA, Smyth MJ, et al. The granzyme
892 B-Serpinb9 axis controls the fate of lymphocytes after lysosomal stress. Cell Death Differ.
893 2014;21(6):876-87.
894 73. Beland M, Desjardins M, Xue D, Mazer BD. Semaphorin 4C Is An Intrinsic Regulator Of Cell-Cell
895 Interaction In Th2 Stimulated Memory-B-Cells. Journal of Allergy and Clinical Immunology.
896 2014;133(2):AB249.
897 74. Szilagyi Z, Gustafsson CM. Emerging roles of Cdk8 in cell cycle control. Biochimica et Biophysica
898 Acta (BBA) - Gene Regulatory Mechanisms. 2013;1829(9):916-20.
899 75. Brackley KI, Grantham J. Activities of the chaperonin containing TCP-1 (CCT): implications for cell
900 cycle progression and cytoskeletal organisation. Cell Stress Chaperones. 2009;14(1):23-31.
901 76. Berry R, Ng N, Saunders PM, Vivian JP, Lin J, Deuss FA, et al. Targeting of a natural killer cell
902 receptor family by a viral immunoevasin. Nat Immunol. 2013;14(7):699-705.
903 77. Bolanos FD, Tripathy SK. Activation receptor-induced tolerance of mature NK cells in vivo
904 requires signaling through the receptor and is reversible. J Immunol. 2011;186(5):2765-71.
905 78. Israr M, DeVoti JA, Papayannakos CJ, Bonagura VR. Role of chemokines in HPV-induced cancers.
906 Seminars in Cancer Biology. 2022;87:170-83.
907 79. Li BH, Garstka MA, Li ZF. Chemokines and their receptors promoting the recruitment of myeloid-
908 derived suppressor cells into the tumor. Mol Immunol. 2020;117:201-15.
909 80. Wang S, Sun Y, Li C, Chong Y, Ai M, Wang Y, et al. TH1L involvement in colorectal cancer
910 pathogenesis by regulation of CCL20 through the NF-κB signalling pathway. J Cell Mol Med.
911 2024;28(10):e18391.
912 81. Ross SH, Cantrell DA. Signaling and Function of Interleukin-2 in T Lymphocytes. Annu Rev
913 Immunol. 2018;36:411-33.

82. Rapp M, Wintergerst MWM, Kunz WG, Vetter VK, Knott MML, Lisowski D, et al. CCL22 controls immunity by promoting regulatory T cell communication with dendritic cells in lymph nodes. J Exp Med. 2019;216(5):1170-81.
83. Jinquan T, Quan S, Feili G, Larsen CG, Thestrup-Pedersen K. Eotaxin activates T cells to chemotaxis and adhesion only if induced to express CCR3 by IL-2 together with IL-4. J Immunol. 1999;162(7):4285-92.
84. Chia TY, Billingham LK, Boland L, Katz JL, Arrieta VA, Shireman J, et al. The CXCL16-CXCR6 axis in glioblastoma modulates T-cell activity in a spatiotemporal context. Front Immunol. 2023;14:1331287.
85. Böttcher JP, Beyer M, Meissner F, Abdullah Z, Sander J, Höchst B, et al. Functional classification of memory CD8+ T cells by CX3CR1 expression. Nature Communications. 2015;6(1):8306.
86. Tu GW, Ju MJ, Zheng YJ, Hao GW, Ma GG, Hou JY, et al. CXCL16/CXCR6 is involved in LPS-induced acute lung injury via P38 signalling. J Cell Mol Med. 2019;23(8):5380-9.
87. Christiani DC. Vaping-Induced Acute Lung Injury. N Engl J Med. 2020;382(10):960-2.
88. Kagohashi K, Sasaki Y, Ozawa K, Tsuchiya T, Kawahara S, Saitoh K, et al. Role of Signal-Transducing Adaptor Protein-1 for T Cell Activation and Pathogenesis of Autoimmune Demyelination and Airway Inflammation. The Journal of Immunology. 2024;212(6):951-61.
89. Zhu X, Guan R, Zou Y, Li M, Chen J, Zhang J, Luo W. Cold-inducible RNA binding protein alleviates iron overload-induced neural ferroptosis under perinatal hypoxia insult. Cell Death & Differentiation. 2024;31(4):524-39.
90. Mikulski Z, Zaslona Z, Cakarova L, Hartmann P, Wilhelm J, Tecott LH, et al. Serotonin activates murine alveolar macrophages through 5-HT2C receptors. Am J Physiol Lung Cell Mol Physiol. 2010;299(2):L272-80.
91. Dutta S, Sengupta P. Men and mice: Relating their ages. Life Sci. 2016;152:244-8.
92. Jackson SJ, Andrews N, Ball D, Bellantuono I, Gray J, Hachoumi L, et al. Does age matter? The impact of rodent age on study outcomes. Lab Anim. 2017;51(2):160-9.
93. Lee YO, Nonnemaker JM, Bradfield B, Hensel EC, Robinson RJ. Examining Daily Electronic Cigarette Puff Topography Among Established and Nonestablished Cigarette Smokers in their Natural Environment. Nicotine Tob Res. 2018;20(10):1283-8.
94. Kaur GR, I. URMC TriState SenNet Mouse Lung Digestion. protocols.io2024.
95. Hao Y, Hao S, Andersen-Nissen E, Mauck WM, 3rd, Zheng S, Butler A, et al. Integrated analysis of multimodal single-cell data. Cell. 2021;184(13):3573-87.e29.
96. Schaum N, Karkanias J, Neff NF, May AP, Quake SR, Wyss-Coray T, et al. Single-cell transcriptomics of 20 mouse organs creates a Tabula Muris. Nature. 2018;562(7727):367-72.
97. Love MI, Huber W, Anders S. Moderated estimation of fold change and dispersion for RNA-seq data with DESeq2. Genome Biology. 2014;15(12):550.
98. Yu G, Wang LG, Han Y, He QY. clusterProfiler: an R package for comparing biological themes among gene clusters. Omics. 2012;16(5):284-7.

Figures:

Figure 1: E-cig aerosols show flavor-dependent changes in the levels of quantified metals

Schematics showing the exposure profile and experimental design to understand the effect of exposure to differently flavored e-cig aerosols in the lungs from C57BL/6J mice using scRNA seq (A) and the nose only exposure system used for performing the mouse experiment (B). The exposure characteristics were assessed by measuring the serum cotinine levels in the blood of exposed and control mice. Data are shown as mean ± SEM (n = 4/group); ns: not significant. **p<0.01, and ***p<0.001 vs air, per one-way ANOVA for multiple comparison (C) and analyzing the levels of metals in the aerosols captured from each day of exposure using ICP-MS (D). Lung morphometric changes as observed using H&E staining of lung slices from air, PGVG and differently flavored e-cig exposed mice. Representative images of n = 2/sex/group at 10X magnification is provided (E) and quantified values for mean linear intercept (Lm) plotted in a sex-specific manner (F)

Figure 2: scRNA seq analyses reveals maximum changes in the cell states of immune cell population upon exposure to differently flavored e-cig aerosols.

Male and female C57BL/6J mice were exposed to 5-day nose-only exposure to differently flavored e-cig aerosols. The mice were sacrificed after the final exposure and lungs from air (control) and differently flavored e-cig aerosol (fruit, menthol, and tobacco)-exposed mice were used to perform scRNA seq. UMAP plot of 71,725 cells captured during scRNA seq showing the four major cell populations identified from control and experimental mouse lungs (A) and the expression of canonical markers used for identifying stromal (*Col3a1*), epithelial (*Sftpa1*), endothelial (*Cldn5*) and immune (*Ptprc*) cell populations. The intensity of expression is indicated by the red-yellow coloring (B). The cell frequencies (plotted as percentage) of different cell clusters

in each sample type showing the sex-dependent variations in the cell composition on exposure to differently flavored e-cig aerosols (C). Bar graphs showing the number of significant DEGs ($p < 0.01$) found to be up (blue) and down (orange)- regulated in each cell cluster in differently flavored e-cig aerosol exposed mouse lungs as compared to air controls as determined by aggregate analyses for both sexes in each group using DESeq2 (D).

Figure 3: Cellular composition of myeloid cells in air and e-cig aerosol exposed mouse lung reveal a unique population of neutrophils.

A total of 14 unique cell clusters were identified from the myeloid cell subset of air and e-cig aerosol exposed mouse lung (A). UMAP plot showing the cell cycle state of different cell types in the myeloid cluster as determined using the Cell cycle scoring in Seurat (B). The heatmap showing the most DEGs in each cluster across the myeloid subset. These differential expressions were used to determine and name the cell types in this cluster. The intensity of expression is indicated by the purple coloring (C). The cell percentages of different cell types in the myeloid cluster showing the sex-dependent variations in the cell composition on exposure to differently flavored e-cig aerosols (D). Flow cytometry results showing sex-dependent changes in the percentages of lung neutrophils (CD45+ CD11b+ Ly6G+) in lung tissue digest (E) and alveolar macrophages (CD45+ CD11b- SiglecF+) in BALF (F) from mice exposed to differently flavored e-cig aerosols. Data are shown as mean ± SEM (n = 3/sex/group). *$p<0.05$, and ****$p<0.0001$, per Tukey post hoc two-way ANOVA comparison.

Figure 4: Exposure to flavored e-cig aerosols result in dampening of neutrophil-mediated innate immune responses in C57BL/6J mouse lungs.

Heatmap and bar plot showing the DESeq2 and GO analyses results respectively from the DEGs in the myeloid cell cluster from Fruit (A & B), menthol (C&D) and tobacco (E&F)-flavored e-cig aerosol exposed mouse lungs as compared to air controls. Heatmap (G) and bar plot (H) showing the DESeq2 and GO analyses results respectively from the DEGs in the Ly6G- neutrophil cluster from air and flavored e-cig (fruit, menthol and tobacco) aerosol exposed mouse lungs.

Figure 5: Exposure to tobacco-flavored e-cig aerosols results in significant increase in lung T-cell percentages in C57Bl/6J mice.

A total of 10 unique cell clusters were identified from the lymphoid cell subset of air and e-cig aerosol exposed mouse lung (A). The heatmap showing the most DEGs in each cluster across the myeloid subset. These differential expressions were used to determine and name the cell types in this cluster. The intensity of expression is indicated by the purple coloring (B). The cell percentages of different cell types in the lymphoid cluster showing the sex-dependent variations in the cell composition on exposure to differently flavored e-cig aerosols (C). Flow cytometry results showing changes in the percentages of lung CD4+ and CD8+ T-cells in the lung tissue digest (D) from mice exposed to differently flavored e-cig aerosols as depicted in a sex-specific manner. Data are shown as mean ± SEM (n = 3/sex/group). *$p<0.05$, **$p<0.01$, and ****$p<0.0001$, per Tukey post hoc two-way ANOVA comparison.

Figure 6: Exposure to tobacco flavored e-cig aerosols result in activation of T-cytotoxic responses in C57BL/6J mouse lungs.

Heatmap and bar plot showing the DESeq2 and GO analyses results respectively from the DEGs in the lymphoid cell cluster from Fruit (A & B), menthol (C&D) and tobacco (E&F)-flavored e-cig aerosol exposed mouse lungs as compared to air controls.

Figure 7: GO analyses of the commonly dysregulated genes show enrichment of dampened innate immune response upon exposure to flavored e-cig aerosols in C57BL/6J mice.

Heat map showing the sex-dependent average fold changes in the levels of cytokines/chemokines in the lung of differently flavored e-cig aerosol exposed C57Bl/6J mouse lungs as compared to air controls. Data are shown as mean ± SEM (n = 3/sex/group) (A). Heatmap showing the fold changes in the expression of commonly dysregulated genes in the myeloid cluster and lymphoid clusters in mouse lungs exposed to flavored e-cig aerosols as compared to ambient air as determined after DESeq2 analyses (B).

CNET plot results showing the pathways regulated by the common DEGs on acute (5-day) exposure to differently flavored fruit, menthol, and tobacco) e-cig aerosols in C57Bl/6J mouse lungs (B).

Tables

Table 1: Table showing the levels of common elements found in the flavored e-liquids and e-cig aerosols in as measured using ICP-MS.

Element	Eliquid; ppb/ mg of eliquid				E-cig Aerosol (Mean ± SD); ppb/ mg of eliquid			
	PGVG	Fruit	Menthol	Tobacco	PGVG	Fruit	Menthol	Tobacco
S	75.63	68.36	95.34	79.79	70.67 ± 16.94	74.05 ± 39.63	81.31 ± 27.24	91.81 ± 11.67
Ni	2.09	1.63	4.73	2.84	1.04 ± 1.00	30.47 ± 14.28	83.52 ± 20.53	41.73 ± 12.25
Cu	2.16	0.87	2.72	2.00	0.37 ± 0.22	1.04 ± 0.48	1.85 ± 0.70	1.32 ± 0.39
Si	1.05	1.13	1.55	1.26	1.10 ± 0.14	1.09 ± 0.35	1.32 ± 0.28	1.33 ± 0.12
K	0.80	0.84	1.21	0.67	0.94 ± 0.13	0.99 ± 0.45	1.32 ± 0.28	0.51 ± 0.10
Na	0.39	0.40	1.10	0.63	0.65 ± 0.11	0.91 ± 0.17	1.70 ± 0.37	0.79 ± 0.11
W	0.48	0.23	0.24	0.14	0.46 ± 0.20	0.30 ± 0.18	0.28 ± 0.14	0.22 ± 0.05
Zn	0.32	0.36	0.68	1.94	0.18 ± 0.01	1.45 ± 0.48	2.06 ± 0.48	1.71 ± 0.42

Ir	0.28	0.47	0.27	0.11	1.19 ± 0.76	0.35 ± 0.29	0.19 ± 0.12	0.14 ± 0.05
B	0.14	0.02	0.02	0.02	0.07 ± 0.02	0.02 ± 0.01	0.02 ± 0.01	0.02 ± 0.01
Ta	0.14	0.34	0.24	0.13	0.73 ± 0.30	0.24 ± 0.09	0.18 ± 0.06	0.13 ± 0.02
Hf	0.13	0.18	0.13	0.07	0.43 ± 0.19	0.14 ± 0.05	0.09 ± 0.03	0.07 ± 0.01
Mo	0.08	0.01	0.01	0.01	0.02 ± 0.01	0.07 ± 0.01	0.15 ± 0.04	0.06 ± 0.02
Pd	0.07	0.14	0.11	0.06	0.30 ± 0.14	0.11 ± 0.06	0.07 ± 0.02	0.06 ± 0.01
Pt	0.05	0.06	0.05	0.07	0.16 ± 0.07	0.09 ± 0.05	0.08 ± 0.04	0.08 ± 0.03
Zr	0.04	0.01	0.02	0.02	0.02 ± 0.01	0.02±0.01	0.01 ± 0.00	0.01 ± 0.00
Sn	0.02	0.06	0.05	0.04	0.06 ± 0.02	0.07 ± 0.02	0.03 ± 0.01	0.03 ± 0.01
Mg	0.01	0.01	0.04	0.03	0.02 ± 0.00	0.12 ± 0.03	0.12 ± 0.03	0.10 ± 0.02
Al	0.01	0.01	0.01	0.01	0.01 ± 0.00	0.01 ± 0.00	0.01 ± 0.00	0.01 ± 0.00
Co	0.01	0.01	0.01	0.01	0.01 ±	0.02 ±	0.03 ±	0.02 ±

					0.00	0.00	0.01	0.00
Nb	0.01	0.00	0.00	0.00	0.01 ± 0.00	0.00 ± 0.00	0.00 ± 0.00	0.00 ± 0.00
Ba	0.01	0.01	0.01	0.01	0.01 ± 0.01	0.01 ± 0.00	0.01 ± 0.00	0.01 ± 0.00
Re	0.01	0.01	0.01	0.02	0.06 ± 0.04	0.03 ± 0.03	0.02 ± 0.01	0.02 ± 0.01

Table 2: DESeq 2 results showing the number of significantly ($p_{adj} < 0.05$) up- or downregulated genes in different cell clusters

Comparisons	**Myeloid Cells**		**Lymphoid Cells**		**Endothelial cells**		**Stromal Cells**		**Epithelial Cells**	
	Up	**Down**	**Up**	**Down**	**Up**	**Down**	**Up**	**Down**	**Up**	**Down**
PGVG vs Air	57	219	9	15	31	20	106	48	17	2
Menthol vs Air	220	104	8	1	59	80	37	14	6	4
Fruit Vs Air	17	7	40	72	3	12	8	2	8	2
Tobacco vs Air	338	215	25	16	87	110	29	13	5	5
Menthol vs PGVG	673	200	55	9	38	87	8	22	4	40
Fruit vs PGVG	135	127	25	12	25	20	29	9	12	12
Tobacco vs PGVG	852	408	90	12	52	87	44	48	5	15

Table 3: Table showing the cell types identified from myeloid and lymphoid clusters and their abbreviations

Cell Types	Abbreviations	Cell Types	Abbreviations
Resident alveolar macrophages	RAM	Rpl+ dendritic cell	Rpl+ DC
Proliferating Alveolar macrophages	pRAM	Plasmacytoid dendritic cell	pDC
Resolving alveolar macrophages	Resolving AM	B-cell progenitors	Pro B cell
Pde3a+ alveolar macrophages	Pde3a+ AM	B-cell precursor	Pre B cell
Interstitial macrophages	IM	Mature B cell	Mature B cell
Classical monocytes	CM	Interferon stimulated B-cell	IFN stim. B cell
Non-classical monocytes	NCM	CD8+ T cell	CD8+ T cell
Dendritic cell 1	cDC1	αβ T cell	αβ T cell
Dendritic cell 2	cDC2	Regulatory T cells	Treg cell
γδ T cell	γδ T cell	Natural Killer cells	NK cell

Table 4: List of top dysregulated genes on exposure to differently flavored (fruit, menthol and tobacco) e-cig aerosol in C57Bl/6J mouse lungs

Genes	Gene Names	Gene Function

Neurl3	Neuralized E3 Ubiquitin Protein Ligase 3	ubiquitin protein ligase activity
Egfem1	EGF-like and EMI domain containing 1	calcium ion binding activity
Stap1	Signal Transducing Adaptor Family Member 1	protein kinase binding and SH3/SH2 adaptor activity
Tfec	Transcription Factor EC	multiple cellular processes including survival, growth and differentiation
Mitf	Melanocyte Inducing Transcription Factor	critical role in cell differentiation
Cirbp	Cold Inducible RNA Binding Protein	role in cold-induced suppression of cell proliferation
Hist1h1c	H1.2 linker histone	functions in the compaction of chromatin
Gmds	GDP-Mannose 4,6-Dehydratase	coenzyme binding and $NADP^+$ binding
Htr2c	5-Hydroxytryptamine Receptor 2C	G protein-coupled receptor activity
Nfia	Nuclear Factor I A	DNA-binding transcription factor activity
Klra8	killer cell lectin-like receptor	carbohydrate binding activity. Acts upstream of or within response to virus
Trp53i11	Tumor Protein P53 Inducible Protein 11	negative regulation of cell population proliferation
Ehd2	EH Domain Containing 2	Angiopoietin-like protein 8 regulatory pathway and response to elevated platelet cytosolic Ca2+.
Ackr2	Atypical Chemokine Receptor 2	recruitment of effector immune cells to the inflammation site.
Marcks	Myristoylated Alanine Rich Protein Kinase C Substrate	involved in cell motility, phagocytosis, membrane trafficking and mitogenesis
Pfkl	Phosphofructokinase,	protein binding and monosaccharide binding

Ramp3	Receptor Activity Modifying Protein 3	signaling receptor activity and coreceptor activity
Chrm3	Cholinergic Receptor Muscarinic 3	cellular responses such as adenylate cyclase inhibition, phosphoinositide degeneration, and potassium channel mediation
Sftpa1	Surfactant Protein A1	carbohydrate binding and lipid transporter activity
Add3	Adducin 3	actin binding and calmodulin binding
Hmgb3	High Mobility Group Box 3	important role in maintaining stem cell populations and may be aberrantly expressed in tumor cells.
Acot1	Acyl-CoA Thioesterase 1	involved in acyl-CoA metabolic process; long-chain fatty acid metabolic process; and very long-chain fatty acid metabolic process
H1f0	H1.0 Linker Histone	Cellular responses to stimuli and Programmed Cell Death.
Scgb3a2	Secretoglobin Family 3A Member 2	secreted lung surfactant protein
Scgb1a1	Secretoglobin Family 1A Member 1	implicated in numerous functions including anti-inflammation, inhibition of phospholipase A2 and the sequestering of hydrophobic ligands
Gpam	Glycerol-3-Phosphate Acyltransferase, Mitochondrial	acyltransferase activity and glycerol-3-phosphate O-acyltransferase activity
Cdh11	Cadherin 11	integral membrane proteins that mediate calcium-dependent cell-cell adhesion.
Ldlr	Low Density Lipoprotein Receptor	cell surface proteins involved in receptor-mediated endocytosis of specific ligands.
Myocd	Myocardin	transcriptional co-activator of serum response factor (SRF)

Table 5: Gene Ontology results showing the top hits from the commonly dysregulated genes in all clusters on exposure to e-cig aerosols

GO ID	**ONTOLOGY**	**Description**	**Gene ID**	**BgRatio**	**p.adjust**
GO:0045907	BP	positive regulation of vasoconstriction	Htr2c/Chrm3/Add3	53/23062	0.033815
GO:00192	BP	regulation of	Htr2c/Chrm3/Add3	86/2306	0.04249

29		vasoconstriction		2	1
GO:1903978	BP	regulation of microglial cell activation	Stap1/Ldlr	16/23062	0.042491
GO:0002683	BP	negative regulation of immune system process	Hmgb3/Gpam/Scgb1a1/Stap1/Ldlr	464/23062	0.042491
GO:0010867	BP	positive regulation of triglyceride biosynthetic process	Gpam/Ldlr	19/23062	0.042491
GO:0042310	BP	vasoconstriction	Htr2c/Chrm3/Add3	109/23062	0.042491
GO:0046889	BP	positive regulation of lipid biosynthetic process	Htr2c/Gpam/Ldlr	110/23062	0.042491
GO:0010866	BP	regulation of triglyceride biosynthetic process	Gpam/Ldlr	25/23062	0.047046
GO:0001919	BP	regulation of receptor recycling	Ldlr/Ramp3	29/23062	0.047046
GO:0007271	BP	synaptic transmission, cholinergic	Htr2c/Chrm3	29/23062	0.047046
GO:0150077	BP	regulation of neuroinflammatory response	Stap1/Ldlr	29/23062	0.047046
GO:0090208	BP	positive regulation of triglyceride metabolic process	Gpam/Ldlr	31/23062	0.047046
GO:0045987	BP	positive regulation of smooth muscle contraction	Chrm3/Myocd	35/23062	0.047046
GO:0097242	BP	amyloid-beta clearance	Ldlr/Myocd	36/23062	0.047046
GO:0040013	BP	negative regulation of locomotion	Htr2c/Mitf/Stap1/Myocd	360/23062	0.047046
GO:0010667	BP	negative regulation of cardiac muscle cell apoptotic process	Acot1/Myocd	37/23062	0.047046
GO:0001881	BP	receptor recycling	Ldlr/Ramp3	40/23062	0.047046
GO:0010664	BP	negative regulation of striated muscle cell apoptotic process	Acot1/Myocd	40/23062	0.047046
GO:0019432	BP	triglyceride biosynthetic process	Gpam/Ldlr	40/23062	0.047046
GO:0035296	BP	regulation of tube diameter	Htr2c/Chrm3/Add3	173/23062	0.047046
GO:0097746	BP	blood vessel diameter maintenance	Htr2c/Chrm3/Add3	173/23062	0.047046
GO:00017	BP	microglial cell activation	Stap1/Ldlr	42/2306	0.04704

74				2	6
GO:1903725	BP	regulation of phospholipid metabolic process	Htr2c/Ldlr	42/23062	0.047046
GO:0035150	BP	regulation of tube size	Htr2c/Chrm3/Add3	174/23062	0.047046

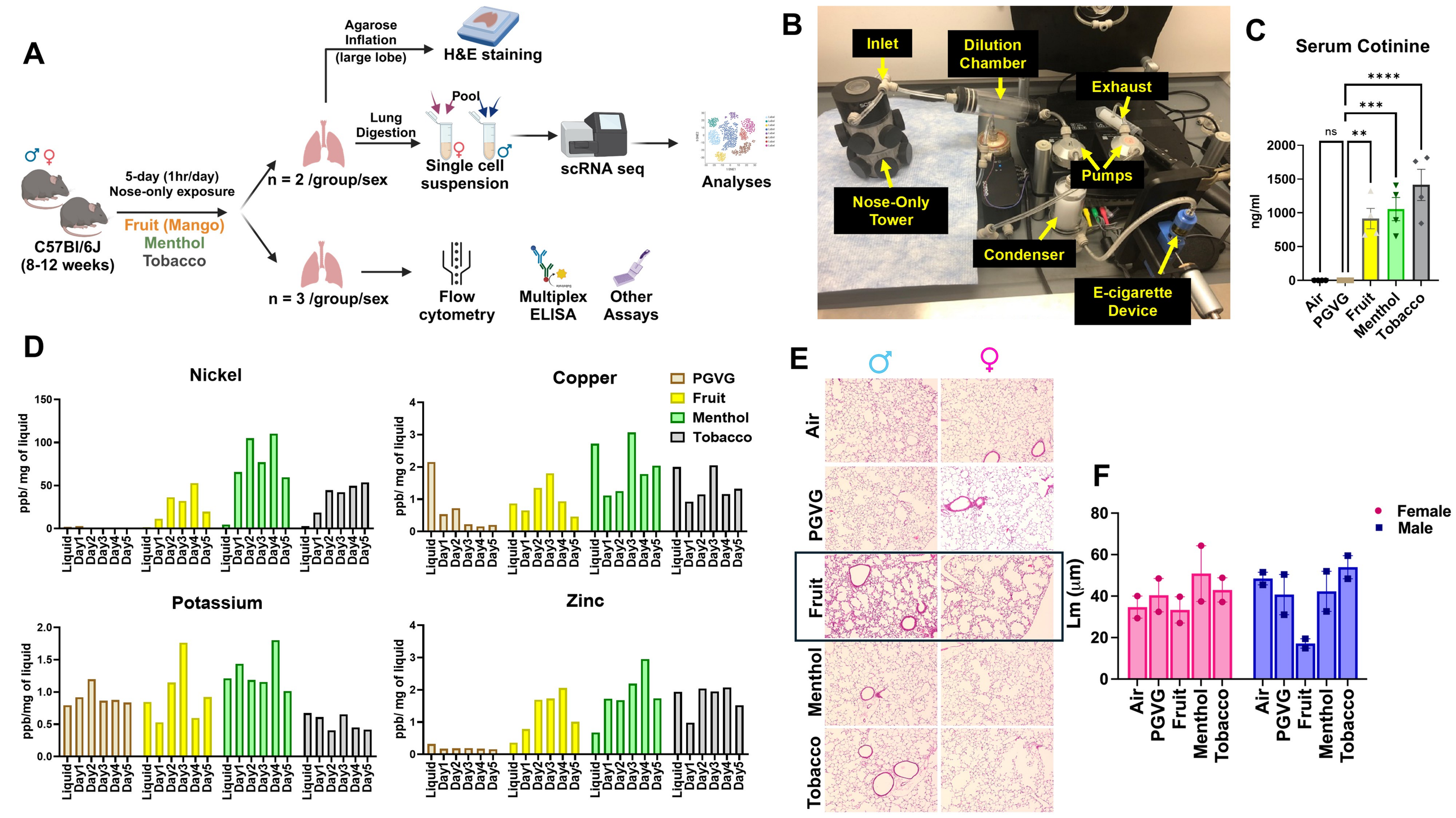
A
Agarose Inflation (large lobe)
H&E staining
Pool
Lung Digestion
Single cell suspension
scRNA seq
Analyses
5-day (1hr/day) Nose-only exposure
Fruit (Mango)
Menthol
Tobacco
C57Bl/6J (8-12 weeks)
n = 2 /group/sex
n = 3 /group/sex
Flow cytometry
Multiplex ELISA
Other Assays
B
Inlet
Dilution Chamber
Exhaust
Pumps
Nose-Only Tower
Condenser
E-cigarette Device
C
Serum Cotinine
ng/ml
ns
**
***
****
Air
PGVG
Fruit
Menthol
Tobacco
D
Nickel
Copper
Potassium
Zinc
ppb/ mg of liquid
PGVG
Fruit
Menthol
Tobacco
Liquid
Day1
Day2
Day3
Day4
Day5
E
Air
PGVG
Fruit
Menthol
Tobacco
F
Lm (μm)
Female
Male

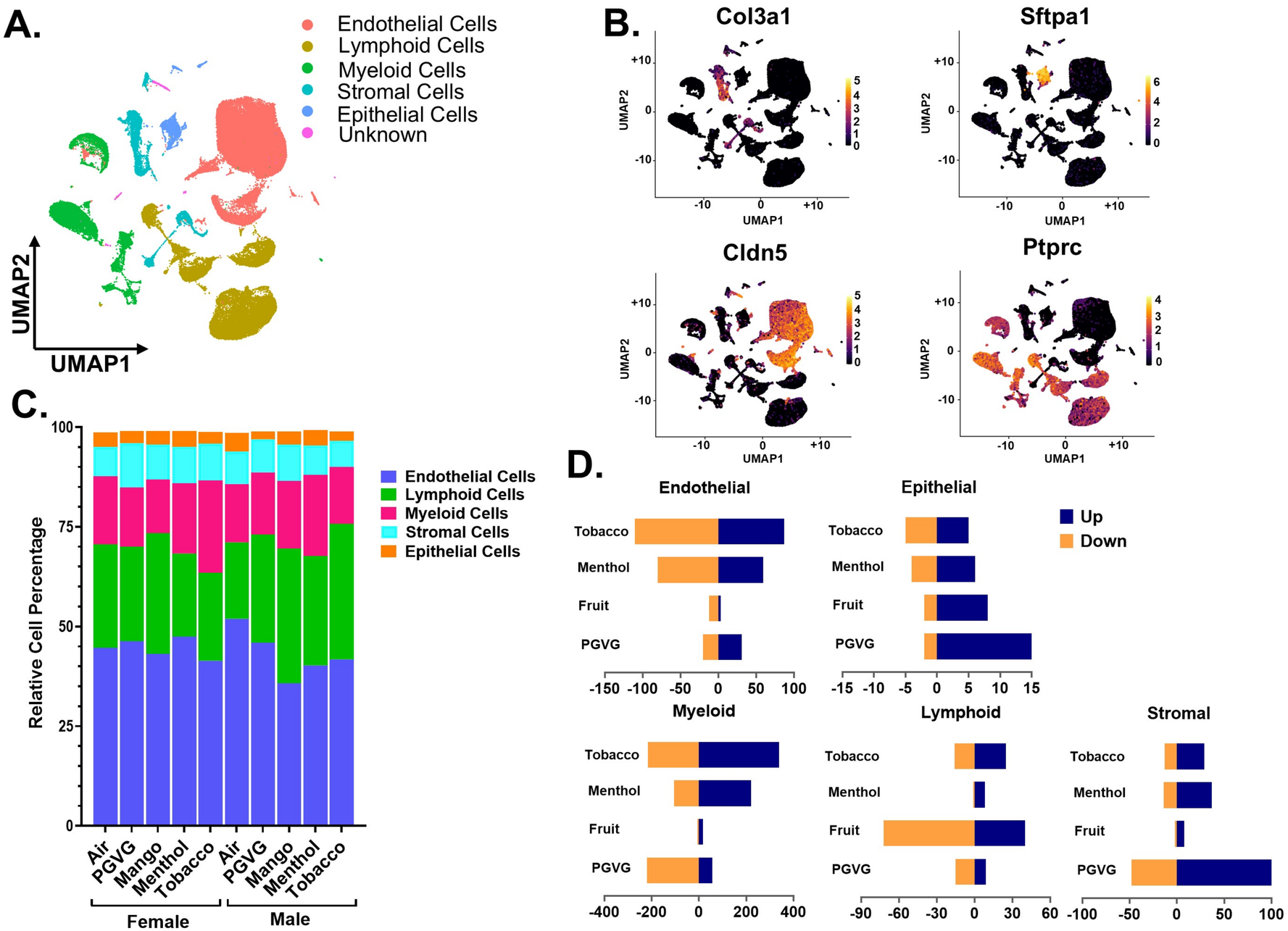
A.
Endothelial Cells
Lymphoid Cells
Myeloid Cells
Stromal Cells
Epithelial Cells
Unknown
UMAP2
UMAP1
B.
Col3a1
Sftpa1
Cldn5
Ptprc
UMAP2
UMAP1
C.
Relative Cell Percentage
Endothelial Cells
Lymphoid Cells
Myeloid Cells
Stromal Cells
Epithelial Cells
Air
PGVG
Mango
Menthol
Tobacco
Female
Male
D.
Endothelial
Epithelial
Myeloid
Lymphoid
Stromal
Up
Down
Tobacco
Menthol
Fruit
PGVG

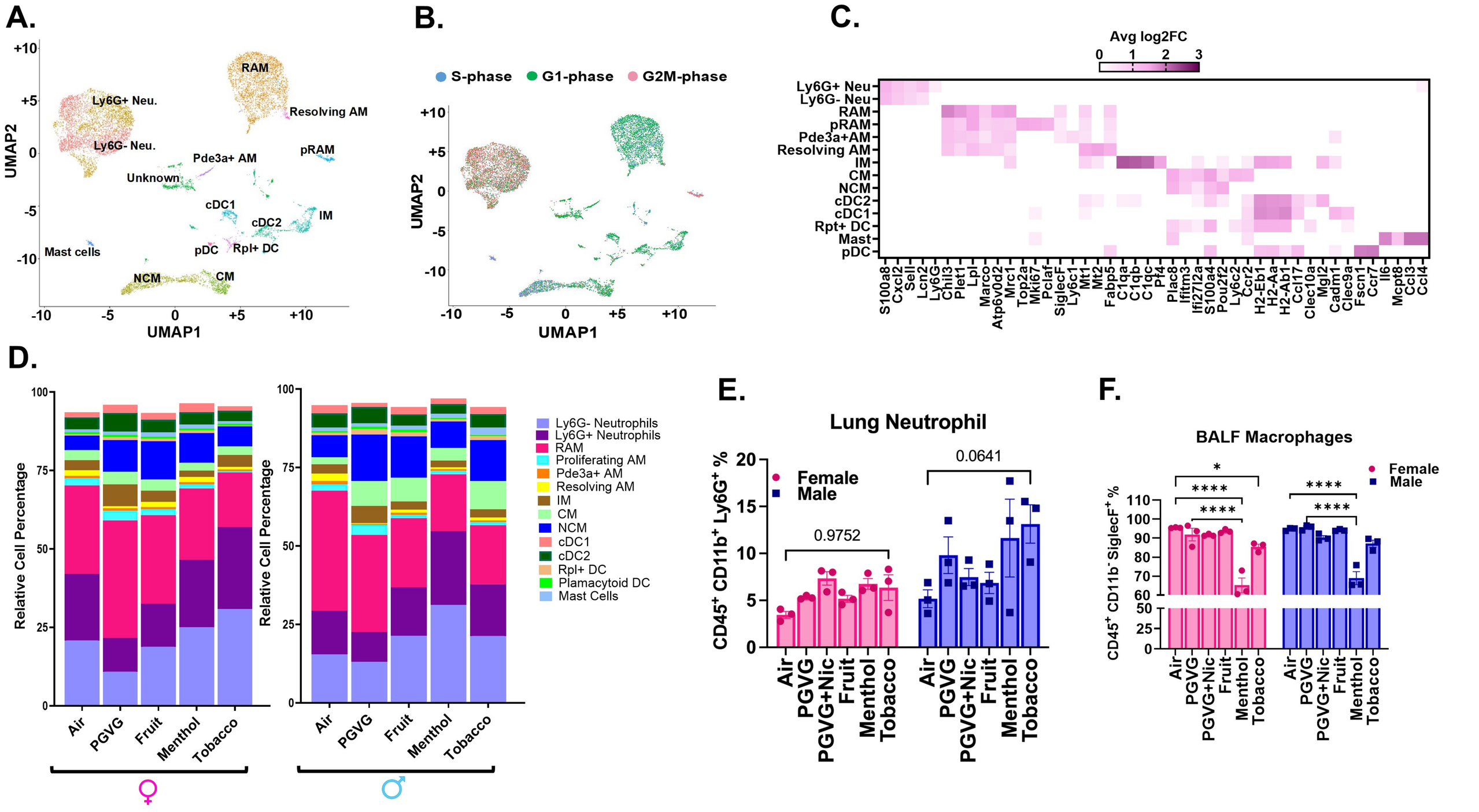
A.
RAM
Ly6G+ Neu.
Resolving AM
Ly6G- Neu.
pRAM
Pde3a+ AM
Unknown
cDC1
cDC2
IM
Mast cells
pDC
Rpl+ DC
NCM
CM
UMAP1
UMAP2
B.
S-phase
G1-phase
G2M-phase
UMAP1
UMAP2
C.
Avg log2FC
Ly6G+ Neu
Ly6G- Neu
RAM
pRAM
Pde3a+AM
Resolving AM
IM
CM
NCM
cDC2
cDC1
Rpt+ DC
Mast
pDC
S100a8
Cxcl2
Sell
Lcn2
Ly6G
Chil3
Plet1
Lpl
Marco
Atp6v0d2
Mrc1
Top2a
Mki67
Pclaf
SiglecF
Ly6c1
Mt1
Mt2
Fabp5
C1qa
C1qb
C1qc
Pf4
Plac8
Ifitm3
Ifi27l2a
S100a4
Pou2f2
Ly6c2
Ccr2
H2-Eb1
H2-Aa
H2-Ab1
Ccl17
Clec10a
Mgl2
Cadm1
Clec9a
Fscn1
Ccr7
Il6
Mcpt8
Ccl3
Ccl4
D.
Relative Cell Percentage
Ly6G- Neutrophils
Ly6G+ Neutrophils
RAM
Proliferating AM
Pde3a+ AM
Resolving AM
IM
CM
NCM
cDC1
cDC2
Rpl+ DC
Plamacytoid DC
Mast Cells
Air
PGVG
Fruit
Menthol
Tobacco
♀
♂
E.
Lung Neutrophil
CD45+ CD11b+ Ly6G+ %
Female
Male
0.9752
0.0641
Air
PGVG
PGVG+Nic
Fruit
Menthol
Tobacco
F.
BALF Macrophages
CD45+ CD11b- SiglecF+ %
Female
Male
*
****
****
****
****
Air
PGVG
PGVG+Nic
Fruit
Menthol
Tobacco

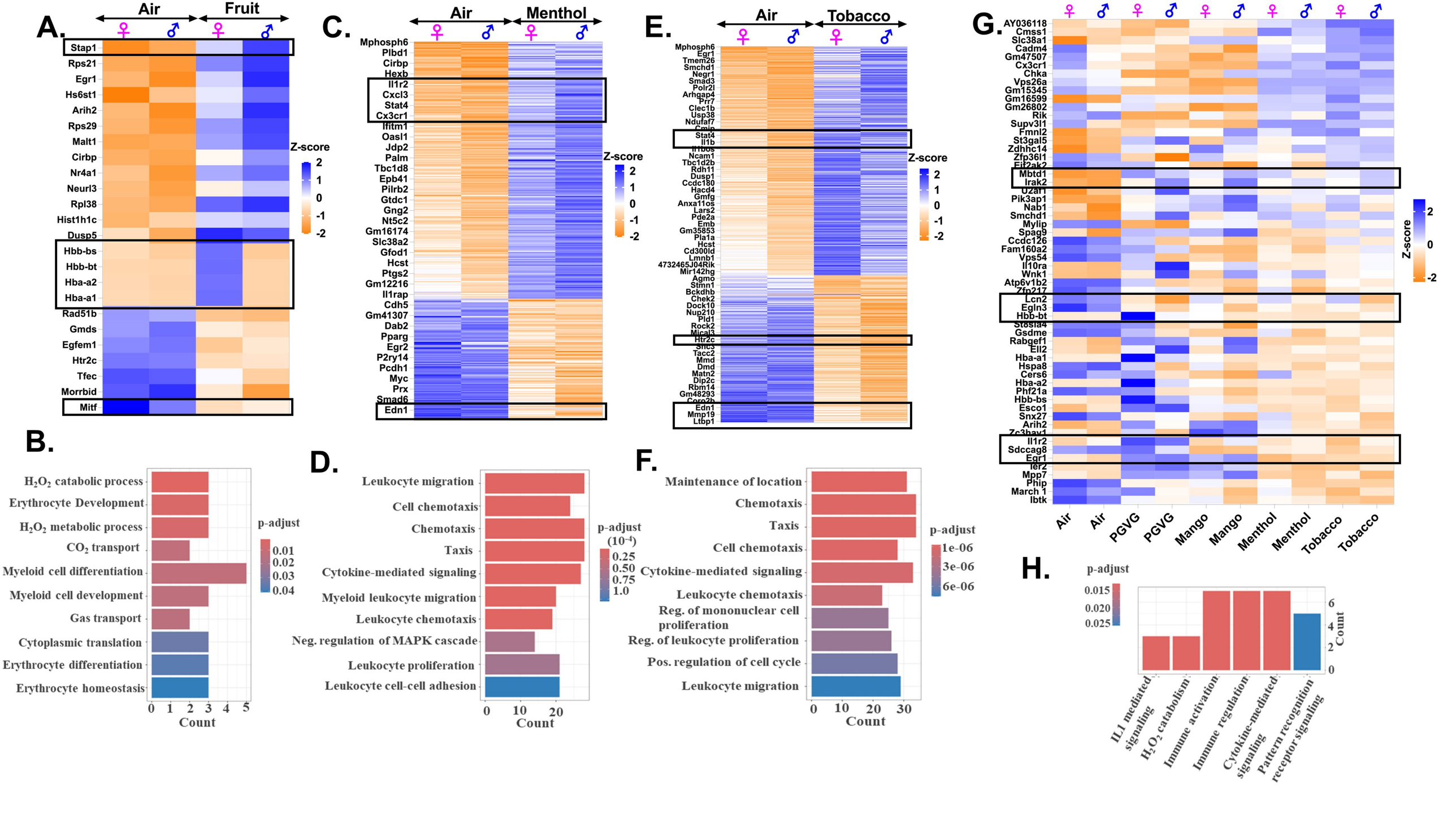
A.
Air
Fruit
Stap1
Rps21
Egr1
Hs6st1
Arih2
Rps29
Malt1
Cirbp
Nr4a1
Neurl3
Rpl38
Hist1h1c
Dusp5
Hbb-bs
Hbb-bt
Hba-a2
Hba-a1
Rad51b
Gmds
Egfem1
Htr2c
Tfec
Morrbid
Mitf
Z-score
2
1
0
-1
-2
B.
H2O2 catabolic process
Erythrocyte Development
H2O2 metabolic process
CO2 transport
Myeloid cell differentiation
Myeloid cell development
Gas transport
Cytoplasmic translation
Erythrocyte differentiation
Erythrocyte homeostasis
0 1 2 3 4 5
Count
p-adjust
0.01
0.02
0.03
0.04
C.
Air
Menthol
Mphosph6
Plbd1
Cirbp
Hexb
Il1r2
Cxcl3
Stat4
Cx3cr1
Ifitm1
Oasl1
Jdp2
Palm
Tbc1d8
Epb41
Pilrb2
Gtdc1
Gng2
Nt5c2
Gm16174
Slc38a2
Gfod1
Hcst
Ptgs2
Gm12216
Il1rap
Cdh5
Gm41307
Dab2
Pparg
Egr2
P2ry14
Pcdh1
Myc
Prx
Smad6
Edn1
Z-score
2
1
0
-1
-2
D.
Leukocyte migration
Cell chemotaxis
Chemotaxis
Taxis
Cytokine-mediated signaling
Myeloid leukocyte migration
Leukocyte chemotaxis
Neg. regulation of MAPK cascade
Leukocyte proliferation
Leukocyte cell-cell adhesion
0 10 20
Count
p-adjust
(10-4)
0.25
0.50
0.75
1.0
E.
Air
Tobacco
Mphosph6
Egr1
Tmem26
Smchd1
Negr1
Smad3
Polr2l
Arhgap4
Prr7
Clec1b
Usp38
Ndufaf7
Cmip
Stat4
Il1b
Ifitm3
Ncam1
Tbc1d2b
Rdh11
Dusp1
Ccdc180
Hacd4
Gmfg
Anxa11os
Lars2
Pde2a
Emb
Gm35853
Pla1a
Hcst
Cd300ld
Lmnb1
4732465J04Rik
Mir142hg
Agmo
Stmn1
Bckdhb
Chek2
Dock10
Nup210
Pld1
Rock2
Mical3
Htr2c
Sftcd
Tacc2
Mmd
Dmd
Matn2
Dip2c
Rbm14
Gm48293
Cace2b
Edn1
Mmp19
Ltbp1
Z-score
2
1
0
-1
-2
F.
Maintenance of location
Chemotaxis
Taxis
Cell chemotaxis
Cytokine-mediated signaling
Leukocyte chemotaxis
Reg. of mononuclear cell proliferation
Reg. of leukocyte proliferation
Pos. regulation of cell cycle
Leukocyte migration
0 10 20 30
Count
p-adjust
1e-06
3e-06
6e-06
G.
AY036118
Cmss1
Slc38a1
Cadm4
Gm47507
Cx3cr1
Chka
Vps26a
Gm15345
Gm16599
Gm26802
Rik
Supv3l1
Fmnl2
St3gal5
Zdhhc14
Zfp36l1
Eif2ak2
Mbtd1
Irak2
Uzaf1
Pik3ap1
Nab1
Smchd1
Mylip
Spag9
Ccdc126
Fam160a2
Vps54
Il10ra
Wnk1
Atp6v1b2
Zfp217
Lcn2
Egln3
Hbb-bt
St8sia4
Gsdme
Rabgef1
Ell2
Hba-a1
Hspa8
Cers6
Hba-a2
Phf21a
Hbb-bs
Esco1
Snx27
Arih2
Zc3hav1
Il1r2
Sdccag8
Egr1
Ier2
Mpp7
Phip
March 1
Ibtk
Air
Air
PGVG
PGVG
Mango
Mango
Menthol
Menthol
Tobacco
Tobacco
Z-score
2
0
-2
H.
p-adjust
0.015
0.020
0.025
Count
6
4
2
0
IL1 mediated signaling
H2O2 catabolism
Immune activation
Immune regulation
Cytokine-mediated signaling
Pattern recognition receptor signaling

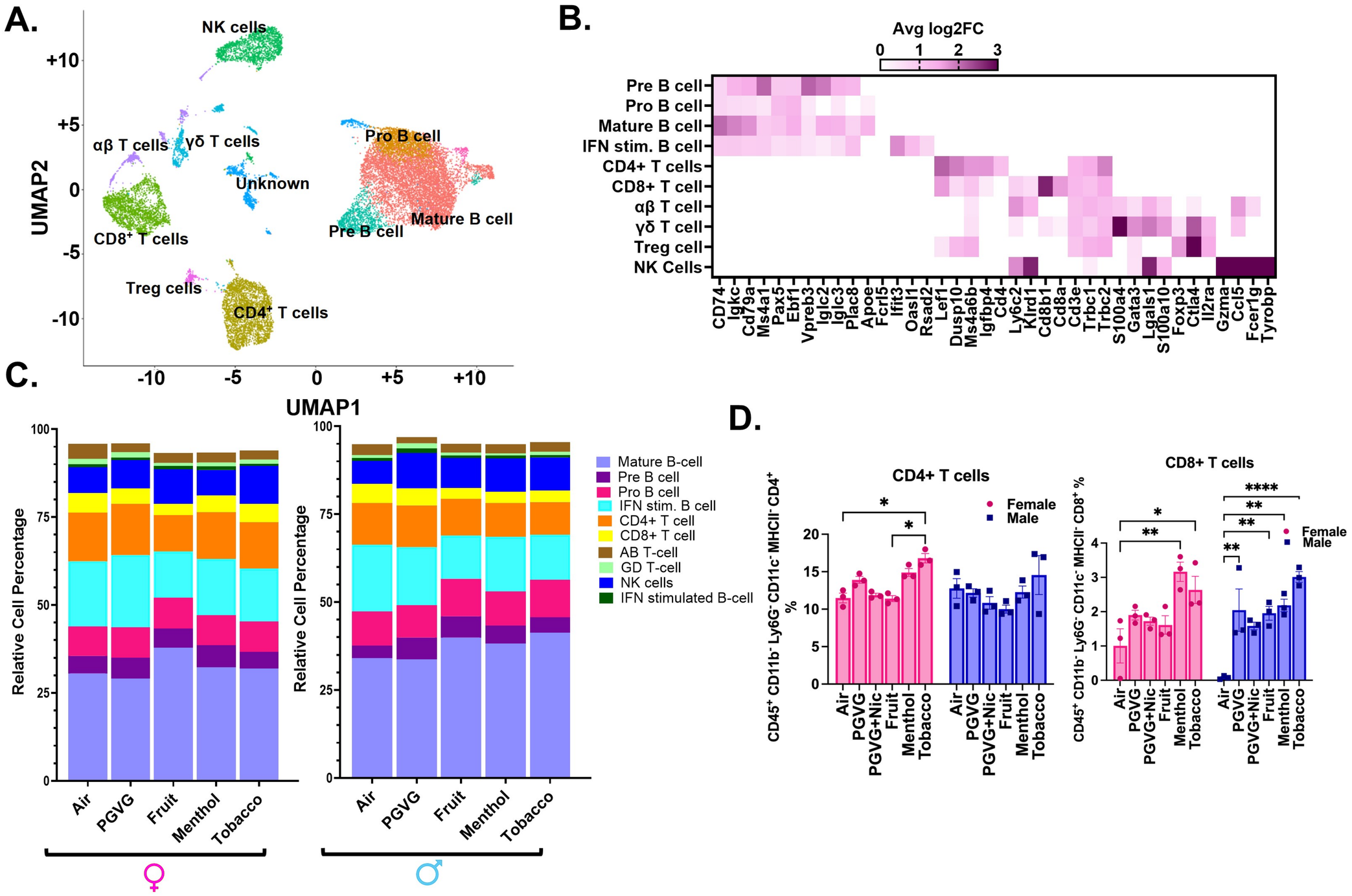
A.
NK cells
αβ T cells
γδ T cells
Unknown
Pro B cell
Mature B cell
Pre B cell
CD8+ T cells
Treg cells
CD4+ T cells
UMAP2
UMAP1
B.
Avg log2FC
Pre B cell
Pro B cell
Mature B cell
IFN stim. B cell
CD4+ T cells
CD8+ T cell
αβ T cell
γδ T cell
Treg cell
NK Cells
CD74
Igkc
Cd79a
Ms4a1
Pax5
Ebf1
Vpreb3
Iglc2
Iglc3
Plac8
Apoe
Fcrl5
Ifit3
Oasl1
Rsad2
Lef1
Dusp10
Ms4a6b
Igfbp4
Cd4
Ly6c2
Klrd1
Cd8b1
Cd8a
Cd3e
Trbc1
Trbc2
S100a4
Gata3
Lgals1
S100a10
Foxp3
Ctla4
Il2ra
Gzma
Ccl5
Fcer1g
Tyrobp
C.
Relative Cell Percentage
Mature B-cell
Pre B cell
Pro B cell
IFN stim. B cell
CD4+ T cell
CD8+ T cell
AB T-cell
GD T-cell
NK cells
IFN stimulated B-cell
Air
PGVG
Fruit
Menthol
Tobacco
D.
CD4+ T cells
CD8+ T cells
Female
Male
PGVG+Nic

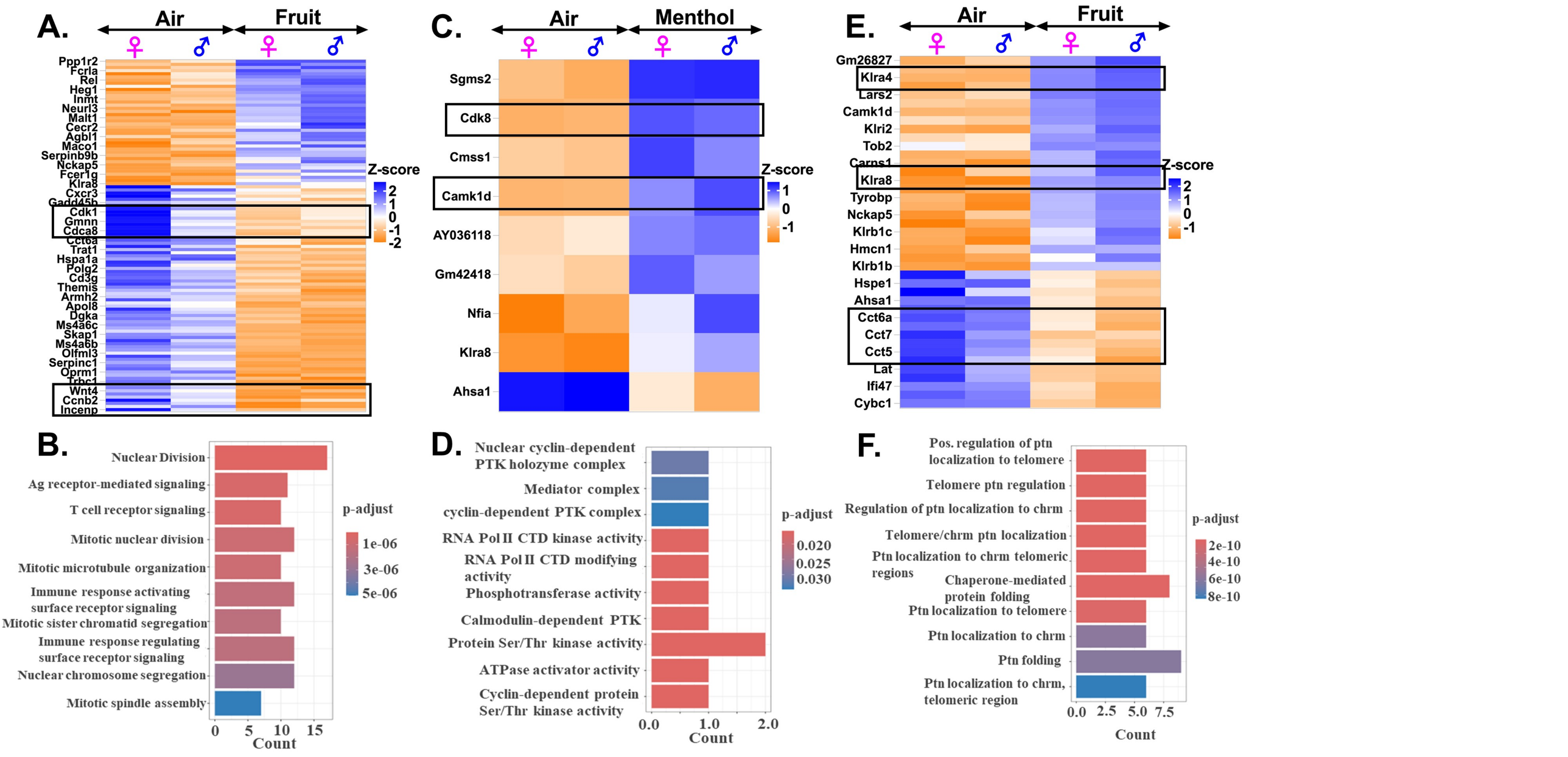
A.
Air
Fruit
♀ ♂ ♀ ♂
Ppp1r2
Fcrla
Rel
Heg1
Inmt
Neurl3
Malt1
Cecr2
Agbl1
Maco1
Serpinb9b
Nckap5
Fcer1g
Klra8
Cxcr3
Gadd45b
Cdk1
Gmnn
Cdca8
Cct6a
Trat1
Hspa1a
Polg2
Cd3g
Themis
Armh2
Apol8
Dgka
Ms4a6c
Skap1
Ms4a6b
Olfml3
Serpinc1
Oprm1
Trbc1
Wnt4
Ccnb2
Incenp
Z-score
2
1
0
-1
-2
C.
Air
Menthol
♀ ♂ ♀ ♂
Sgms2
Cdk8
Cmss1
Camk1d
AY036118
Gm42418
Nfia
Klra8
Ahsa1
Z-score
1
0
-1
E.
Air
Fruit
♀ ♂ ♀ ♂
Gm26827
Klra4
Lars2
Camk1d
Klri2
Tob2
Carns1
Klra8
Tyrobp
Nckap5
Klrb1c
Hmcn1
Klrb1b
Hspe1
Ahsa1
Cct6a
Cct7
Cct5
Lat
Ifi47
Cybc1
Z-score
2
1
0
-1
B.
Nuclear Division
Ag receptor-mediated signaling
T cell receptor signaling
Mitotic nuclear division
Mitotic microtubule organization
Immune response activating surface receptor signaling
Mitotic sister chromatid segregation
Immune response regulating surface receptor signaling
Nuclear chromosome segregation
Mitotic spindle assembly
0
5
10
15
Count
p-adjust
1e-06
3e-06
5e-06
D.
Nuclear cyclin-dependent PTK holozyme complex
Mediator complex
cyclin-dependent PTK complex
RNA Pol II CTD kinase activity
RNA Pol II CTD modifying activity
Phosphotransferase activity
Calmodulin-dependent PTK
Protein Ser/Thr kinase activity
ATPase activator activity
Cyclin-dependent protein Ser/Thr kinase activity
0.0
1.0
2.0
Count
p-adjust
0.020
0.025
0.030
F.
Pos. regulation of ptn localization to telomere
Telomere ptn regulation
Regulation of ptn localization to chrm
Telomere/chrm ptn localization
Ptn localization to chrm telomeric regions
Chaperone-mediated protein folding
Ptn localization to telomere
Ptn localization to chrm
Ptn folding
Ptn localization to chrm, telomeric region
0.0
2.5
5.0
7.5
Count
p-adjust
2e-10
4e-10
6e-10
8e-10

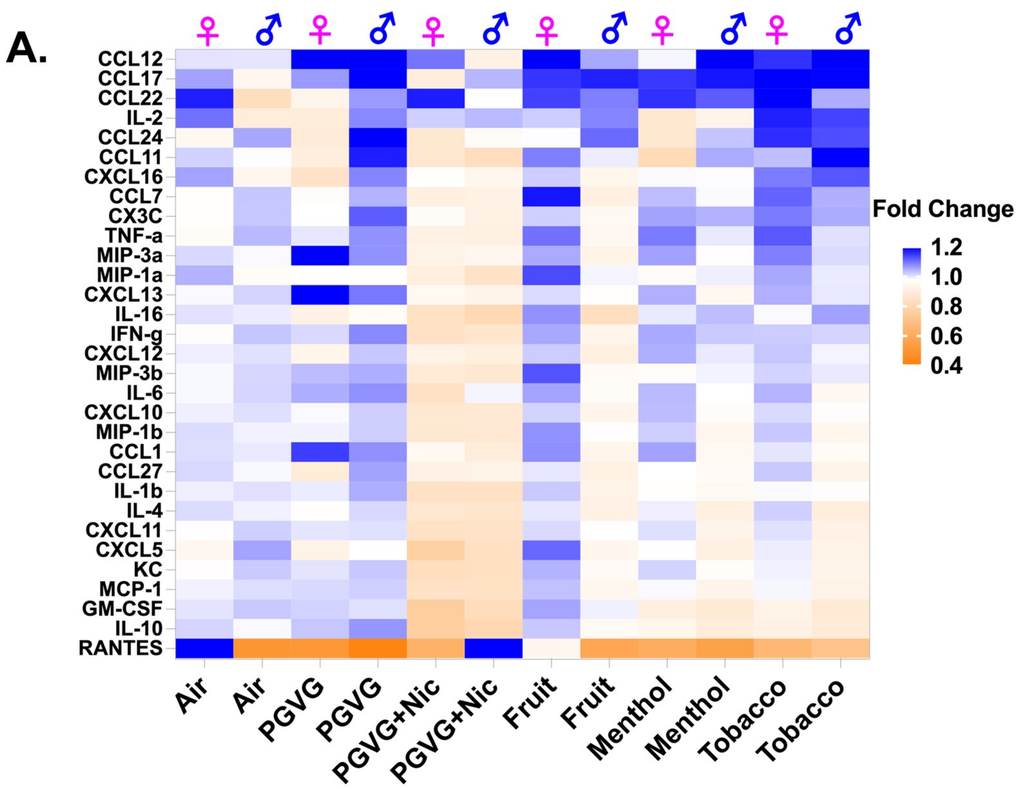
A.
CCL12
CCL17
CCL22
IL-2
CCL24
CCL11
CXCL16
CCL7
CX3C
TNF-a
MIP-3a
MIP-1a
CXCL13
IL-16
IFN-g
CXCL12
MIP-3b
IL-6
CXCL10
MIP-1b
CCL1
CCL27
IL-1b
IL-4
CXCL11
CXCL5
KC
MCP-1
GM-CSF
IL-10
RANTES
Air
Air
PGVG
PGVG
PGVG+Nic
PGVG+Nic
Fruit
Fruit
Menthol
Menthol
Tobacco
Tobacco
Fold Change
1.2
1.0
0.8
0.6
0.4

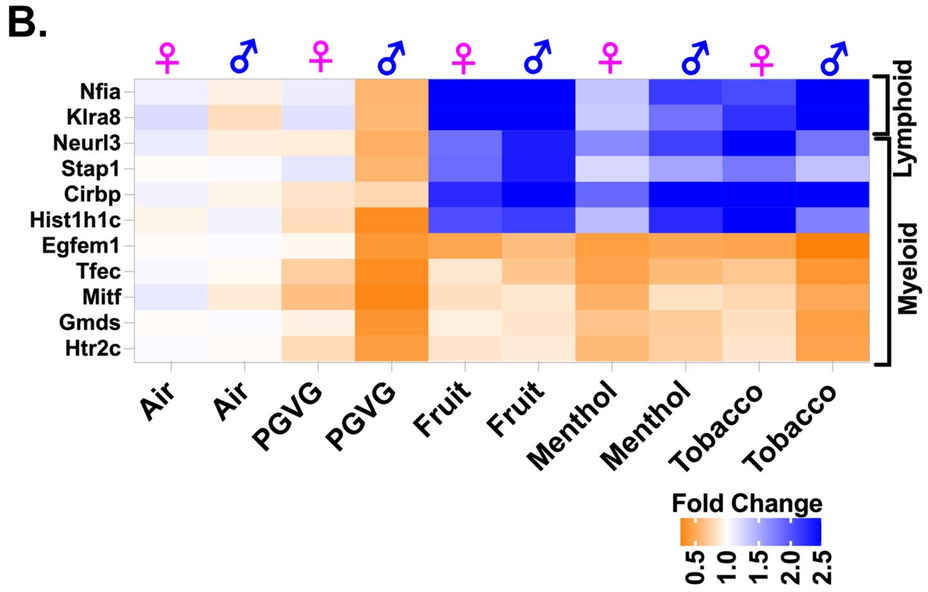
B.
Nfia
Klra8
Neurl3
Stap1
Cirbp
Hist1h1c
Egfem1
Tfec
Mitf
Gmds
Htr2c
Lymphoid
Myeloid
Air
Air
PGVG
PGVG
Fruit
Fruit
Menthol
Menthol
Tobacco
Tobacco
Fold Change
0.5
1.0
1.5
2.0
2.5

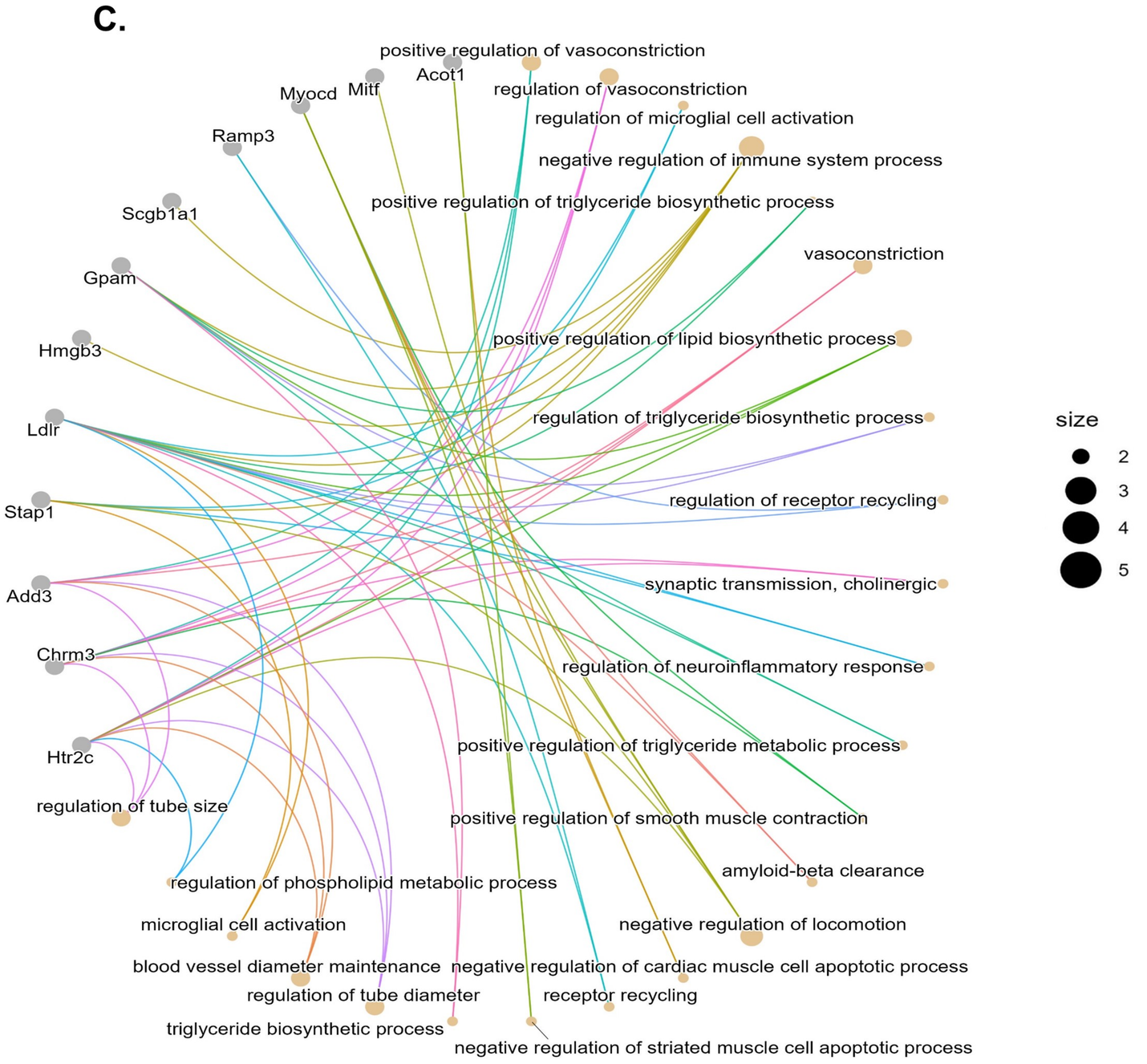
C.
positive regulation of vasoconstriction
Acot1
Mitf
Myocd
regulation of vasoconstriction
regulation of microglial cell activation
Ramp3
negative regulation of immune system process
positive regulation of triglyceride biosynthetic process
Scgb1a1
vasoconstriction
Gpam
positive regulation of lipid biosynthetic process
Hmgb3
regulation of triglyceride biosynthetic process
Ldlr
regulation of receptor recycling
Stap1
synaptic transmission, cholinergic
Add3
regulation of neuroinflammatory response
Chrm3
positive regulation of triglyceride metabolic process
Htr2c
regulation of tube size
positive regulation of smooth muscle contraction
amyloid-beta clearance
regulation of phospholipid metabolic process
negative regulation of locomotion
microglial cell activation
blood vessel diameter maintenance
negative regulation of cardiac muscle cell apoptotic process
regulation of tube diameter
receptor recycling
triglyceride biosynthetic process
negative regulation of striated muscle cell apoptotic process
size
2
3
4
5